SERDP FINAL REPORT

Development of Laser-Based Sensors for VOC/NOx and Metals Emissions Monitoring

CP-1060

Strategic Environmental Research
and Development Program
U.S. Department of Defense

December 2000

Report Documentation Page

Form Approved
OMB No. 0704-0188

1. REPORT DATE	2. REPORT TYPE	3. DATES COVERED
DEC 2000		**00-00-2000 to 00-00-2000**

4. TITLE AND SUBTITLE	5a. CONTRACT NUMBER
Development of Laser-Based Sensors for VOC/NOx and Metals Emissions Monitoring	5b. GRANT NUMBER
	5c. PROGRAM ELEMENT NUMBER
6. AUTHOR(S)	5d. PROJECT NUMBER
	5e. TASK NUMBER
	5f. WORK UNIT NUMBER
7. PERFORMING ORGANIZATION NAME(S) AND ADDRESS(ES) **Sandia National Laboratories,Livermore,CA,94550**	8. PERFORMING ORGANIZATION REPORT NUMBER
9. SPONSORING/MONITORING AGENCY NAME(S) AND ADDRESS(ES)	10. SPONSOR/MONITOR'S ACRONYM(S)
	11. SPONSOR/MONITOR'S REPORT NUMBER(S)

12. DISTRIBUTION/AVAILABILITY STATEMENT
Approved for public release; distribution unlimited

13. SUPPLEMENTARY NOTES

14. ABSTRACT

15. SUBJECT TERMS

16. SECURITY CLASSIFICATION OF:			17. LIMITATION OF ABSTRACT	18. NUMBER OF PAGES	19a. NAME OF RESPONSIBLE PERSON
a. REPORT **unclassified**	b. ABSTRACT **unclassified**	c. THIS PAGE **unclassified**	**Same as Report (SAR)**	**56**	

Check Off
BS S
JM
RH

Development of Laser-Based Sensors for VOC/NOx and Metals Emissions Monitoring
CP 1060-97
Final Report

Scott E. Bisson
Sandia National Laboratories
Livermore CA, 94550

Meng-Dawn Cheng
Oak Ridge National Laboratory
Oak Ridge, Tennessee 37831-6038.

CONTENTS

INTRODUCTION **4**

Objectives 4

Technical Approach. 4

VOC-NO_X DETECTION CHANNEL **6**

FY99 Progress 6

LASER **7**

Source Requirements 7

Laser System 7

Tuning Strategies 9

Continuous tuning 11

PHOTOACOUSTIC SPECTROSCOPY **14**

Background 14

Cell Design 16

Cell Calibration 19

SPECTROMETER **21**

System Characterization 22

FIELD TEST **25**

Issues 25

Field Demonstration 28

Field Measurements 31

Error Analysis 38

FUTURE WORK **40**

Gas Phase Detection 40

ACKNOWLEDGMENTS **41**

REFERENCES **42**

LIPS EXECUTIVE SUMMARY **43**

BACKGROUND **44**

LASER-INDUCED PLASMA SPECTROSCOPY **45**

Experimental Setup 46

High-Resolution Spectrum Obtained via the SERDP ABF-LIPS Technique.....47
Aerosol Beam Focusing Nozzle.....48
Effects of Aerosol Beam Focusing Configuration on LIPS.....49
Selection of Optimal laser Wavelength on ABF-LIPS.....50
Effects of Chemical Speciation on ABF-LIPS.....51

CONCLUSIONS.....52

REFERENCES.....52
ACCOMPLISHMENTS IN FY1999.....54
ACKNOWLEDGMENTS.....55

Introduction

Objectives

This report summarizes our progress during the third and final year of this project. For completeness, a review of the technology and summary of progress during the first and second year are also given. This project addresses the growing compliance monitoring needs of the Department of Defense (DoD) and Department of Energy (DOE) as mandated by both state and federal legislation. Specifically, the Clean Air Act Amendments (CAAA) of 1990 call for the regulation and monitoring of some 189 species which occur in both gas and condensed (aerosol) phases. Of particular importance are volatile organic compounds as they are known to play an important role in the photochemical production of ozone and peroxy acetyl nitrate (PAN), species which pose a major threat to human health. Toxic metals such as mercury and chromium are also important since they are used in many industrial processes and are also a threat to health and safety.

The goal of this work is to develop novel technologies to help meet the compliance monitoring needs of the DoD, DOE and EPA. Specifically, new technology is required to increase the number of species which can be detected, the sensitivity and speed of detection and also to lower costs through increased automation and compact size. Given the wide range of physical properties (aerosol and gas phase) of the CAAA pollutants more than one monitoring technology will be required. This project is divided into two pieces: the development of a novel gas phase monitoring system led by Sandia National Laboratories, Livermore and a metals emissions monitoring system employing novel laser and microspectrometer technology which is led by Oak Ridge National Laboratory. This work will culminate with field testing of the two instruments.

Technical Approach

The gas-phase portion of the system utilizes infrared (IR) absorption spectroscopy to detect analytes of interest. The IR absorption spectra of air samples are determined using laser photoacoustic spectroscopy (PAS), in which a sensitive microphone is used to sense the acoustic wave produced by laser energy deposited in the gas-phase molecules. PAS can detect absorptions as small as 1 part in 10^7, allowing detection of many species at ppb levels. A schematic of the prototype photoacoustic spectrometer is shown in figure 1. The major components of this system are the Nd:YAG pump laser, the tunable infrared OPO, photoacoustic cell and a laptop computer. Our approach to PAS differs from earlier work in its use of a new development in tunable IR lasers. The new technology, termed quasi-phasematching (QPM), makes it possible to develop nonlinear

optical materials whose performance exceeds that of conventional crystals by over an order of magnitude. The idea of quasi-phase matching is not new; it dates back to 1962 but methods for manufacturing QPM materials had not yet been developed. Within the last 5 years however, methods for manufacturing QPM materials based on lithium niobate ($LiNbO_3$) have been developed using photolithographic techniques borrowed from the semiconductor industry. Quasi-phasematched lithium niobate differs from bulk lithium niobate in that the optical axis of the crystal is periodically reversed or poled. When pumped by the fundamental of an Nd:YAG laser, periodically-poled lithium niobate (PPLN) offers the possibility of broad spectral coverage over the mid-infrared region with unprecedented performance. Through a nonlinear coupling between the pump laser and the PPLN crystal, the pump light is split into two *tunable* wavelengths (termed the signal and idler) which are determined by the period of the domain reversal of the crystal and the pump wavelength. By manufacturing PPLN crystals with varying periods broad tuning can be achieved.

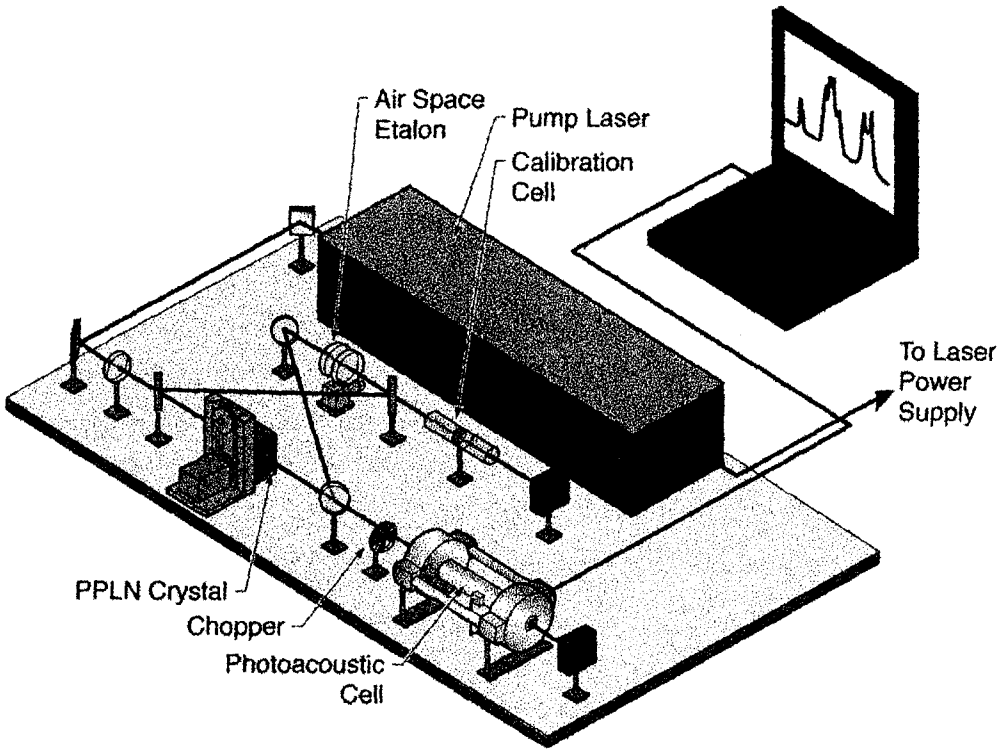

Figure 1. Schematic of the prototype breadboard spectrometer.

The use of periodically-poled lithium niobate (PPLN) in laser devices is growing quickly. PPLN's high nonlinearity, long interaction length, and the ability to *engineer*

the poled structure (and hence the spectral properties) using a photolithographic mask make it an attractive nonlinear material for many applications. By controlling the poled regions through photolithography, a single crystal can be engineered for many different frequency mixing applications. Currently crystals with as many as eight discrete poled regions or with continuously varying periods are commercially available. The high nonlinearity and long interaction length brings the efficiency of many nonlinear frequency conversion techniques to the point where they are suitable for spectroscopy using small lasers. For example, recent work in our laboratory and other labs have demonstrated generation of greater than 30 μWatts of power through difference frequency (DFG) conversion using two 0.5 W diode lasers.[1,2] This amount of DFG power is enough for techniques such as wavelength modulation and frequency modulation spectroscopy. Another application of PPLN's high nonlinearity and long interaction length is the successful demonstration of a cw singly resonant optical parametric oscillator (SRO) pumped with the relatively low threshold of 3 W.[3] Pump powers as low as 800 mW have been used to pump a PPLN SRO when both the pump and signal are resonated.[4] The use of PPLN in OPOs is described in detail in ref. 5.

We have employed PPLN in a compact IR optical parametric oscillator (OPO — a type of laser) that allows continuous breadth of tuning (1.3-4.5 μm) and output power (~200 mW) that were not attainable in a fieldable package in the past. High output power is required to attain the PAS sensitivities required in regulatory applications such as ambient air monitoring or stack monitoring. Continuous tuning reduces ambiguity in spectral identification and discrimination against background materials. Operation in the 1.3 to 4.5 μm range allows detection of many organic effluents, as it encompasses the range in which C-H bonds absorb. The primary existing competitors to this technology are (1) the CO_2 laser, which is only discretely tunable over ~50 lines in the 9-11 μm spectral range, and (2) OPO's based on conventional nonlinear materials, which are tabletop-sized systems that are not conducive to operation in a field environment.

VOC-NO_x Detection Channel

FY99 Progress

We have now completed our third and final year of this project. Our efforts were focused primarily on integrating the laser system with the photoacoustic cell and computer system, evaluation of system performance, characterization of the VOC emission source using GCMS methods, and completion of field testing. Although tuning of the laser was demonstrated during the second year, some efforts were made to further improve the tuning. We have also spent considerable effort characterizing the

photoacoustic cell (responsivity, gas flow, etc..). The following describes each of the above tasks.

Laser

Source Requirements

The choice of photoacoustic spectroscopy as the detection method and the need to detect a broad range of species places certain requirements on the laser. First, to be sensitive it should be cw and capable of an output of a few hundred mWatts or more and second, broad tunability is essential. Other obvious requirements are compactness, high efficiency and ruggedness for field operation. In addition to broad tunability, the optimum wavelength range is in the 3-5μm range where many functional groups such as C-H absorb or in the 8-12 μm range where atmospheric transmission is good and absorptions are strong. These requirements are best satisfied through the use of an OPO based on PPLN. The high nonlinearity, long interaction length, and the ability to engineer the poled structure using a photolithographic mask make PPLN an attractive nonlinear material for many applications. The high nonlinearity and long interaction length brings the efficiency of many nonlinear frequency conversion techniques to the point where they are suitable for spectroscopy using small lasers. Under funding from the Gas Research Institute (GRI) and SERDP we have demonstrated efficient cw, single frequency operation of a PPLN OPO. Outputs as high as several hundred milliwatts with several hundred wavenumbers of coarse tuning in the 3μm region have been routinely obtained. While coarse tuning of a PPLN OPO over a broad spectral range has been demonstrated, fine tuning over a broad spectral range has not yet been demonstrated. Fine tuning is desirable for many spectroscopic and chemical sensing applications. During the second year of this project we have focused on the fine tuning capability of the OPO and have made significant progress towards this goal. The following describes the laser system and our tuning approaches.

Laser System

A schematic of the laser system is shown in figure 2. The basic configuration of the OPO was a bow-tie ring geometry employing a fan type PPLN crystal. This design was discussed in a previous paper.[6] The ring configuration provided better frequency stability, single mode operation and more space for intra-cavity tuning elements than a linear cavity. The OPO cavity was formed by two concave mirrors, R=10cm, with the PPLN crystal in between and two flat mirrors forming the outside leg of the ring. The

curved mirrors were coated on both sides for high transmission (>98%) of the pump beam at 1.064 μm and for high reflectivity (>99.5%) on the curved surfaces at 1.57 μm.

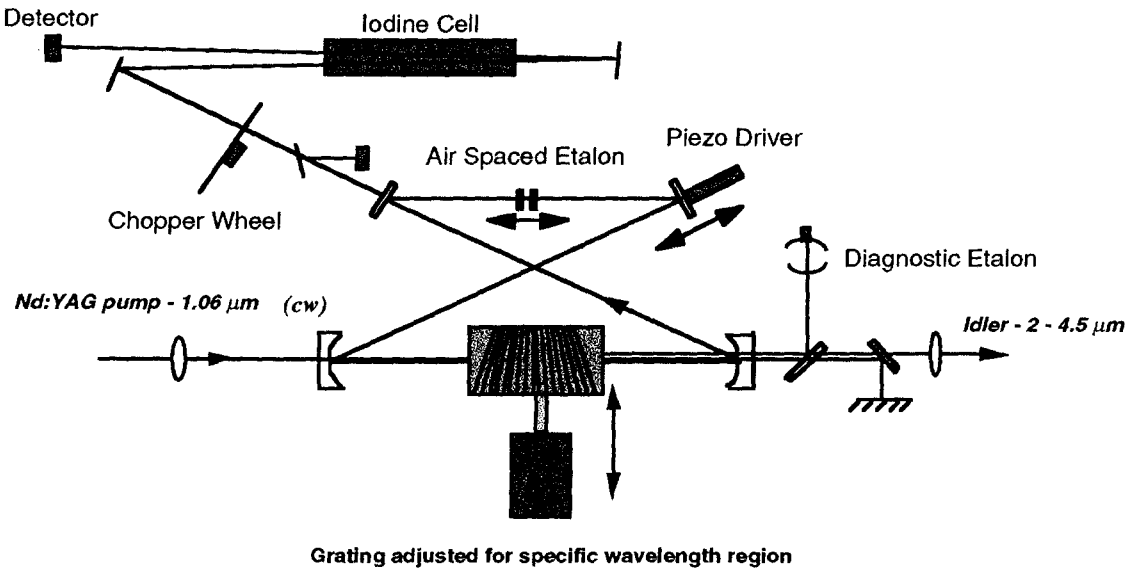

Figure 2. Schematic diagram of the cw ring OPO used in this work.

The reflectivity at 3.0 μm was made as low as possible to avoid idler feedback and to couple as much 3.0 μm light out of the cavity as possible. We have found that with the ring geometry the oscillating mode tends to operate *single* mode or single frequency even without intra-cavity tuning elements. This was not the case with a linear resonator where random mode hopping and multi-mode operation were frequent. In this cavity we resonate the 1.5 μm signal wave and couple out the 3 μm idler wave. It is preferable to resonate the 3μm idler wave but due to mirror coating considerations it is easier to resonate the 1.5μm signal wave.

The OPO was pumped by a cw, single-longitudinal-mode, diode-pumped 6 watt Nd:Vanadate laser manufactured by Coherent Inc. Single mode operation of the pump laser was necessary for achieving single frequency operation at 3.0 μm since the idler spectrum mirrored that of the pump spectrum. A multi-mode pump could be used if the idler wave were resonated inside the OPO cavity instead of the signal wave. However, as discussed above this is difficult due to mirror coating considerations. The pump beam was focused to approximately 100μm in diameter (intensity 10-90% power points) inside the PPLN crystal. The oscillation threshold was approximately 3 watts and when pumped at full power (6.5watts) a pump depletion of 85-90% could be achieved.

The PPLN crystal was of the fan type as shown in figure 3 with periods ranging from 29.3 μm to 30.1 μm. This yielded a coarse tuning range of approximately 350 cm^{-1} from 1.53 to 1.62 μm in the signal and 3.1 μm to 3.5 μm in the idler. The crystal dimensions were 50 mm long, 20 mm wide, and 0.5 mm thick. A 1° wedge between the input and output facets helped to eliminate idler feedback in the OPO. The faces of the PPLN crystal were anti-reflection coated at both 1.064 μm and also at 1.57 μm. To avoid photorefractive damage the crystal was heated in an oven to 130C.

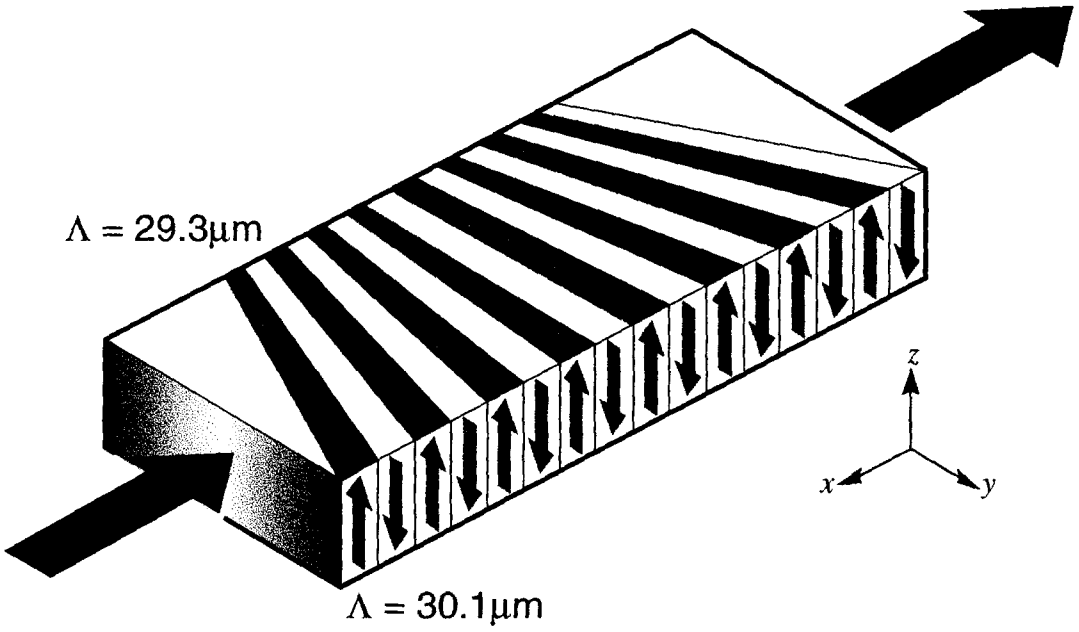

Figure 3. Exaggerated view of the fan-out pattern on the PPLN crystal. Arrows within the crystal indicate the poling direction. For the OPO, the pump, signal, and idler beams are polarized along the crystallographic z-axis (as indicated by the coordinates in the figure), and they propagate along the x-axis (as indicated by the large arrows entering and leaving the crystal), sampling only one periodicity.

Tuning Strategies

We have pursued two tuning strategies for the OPO; mode-hop tuning and continuous tuning. In the mode-hop tuning approach, an intra-cavity etalon was used to control on which longitudinal mode or frequency the OPO oscillated. The basic cavity configuration was similar to the continuous tuning approach as shown in figure 2 except that the etalon could be either an air-spaced or a rotating solid etalon. As will be shown, the tuning characteristics of the two types of etalons are very different. In the case of a solid etalon, tuning over a few wavenumbers could be achieved by rotating the etalon over a few degrees. Although the rotation was nearly continuous, the frequency steps

were discrete on the order of .02-.1 cm^{-1}, depending on the number of cavity modes jumped. The required finesse of the etalon or spectral rejection was actually quite low on the order of a few percent or so. The solid etalon which worked best in our setup was a 400 μm thick, uncoated YAG substrate. The tuning range of the etalon was limited by walkoff losses within the etalon and also by the gain bandwidth of the PPLN crystal. These factors combined to give a mode-hop tuning range of approximately 4 cm^{-1}. Figure 4 shows several scans obtained by mode-hop tuning of the OPO. Although it may

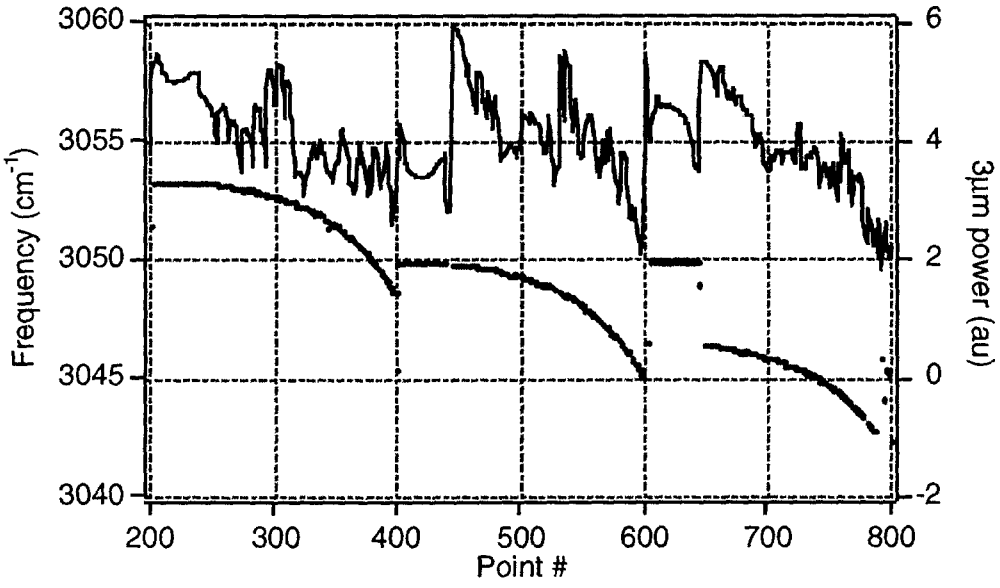

Figure 4. Rotating etalon scan with a 400μm thick solid YAG etalon. Note the quadratic dependence of frequency on tuning (etalon rotation) and also on 3μm power. For this scan, the PPLN crystal was translated synchronously with the etalon which resulted in each etalon scan being displaced from the previous scan. In this way, a broad spectral range can be covered. The jump near point 600 is an etalon mode hop.

appear that an arbitrarily small frequency step can be obtained by a small rotation of the etalon this was not the case. The step size was limited by the optical length of the cavity (the free spectral range) which for this system was approximately 580 MHz. For most atmospherically broadened species which have a linewidths on the order of a few GHz this mode spacing is small enough to resolve most spectral features. To achieve scans larger than 4 cm^{-1} the PPLN crystal was translated approximately .04 mm which moved the OPO gain peak approximately 4 cm^{-1}. This method of tuning is attractive in that it is simple, employing only an intra-cavity etalon and no lock-loops or feedback circuits. There are several drawbacks however, of using a rotating solid etalon. First, as is evident

from figure 4, the scan rate depends nonlinearly (quadratically) on etalon angle which requires software to linearize the scan and furthermore, the intra-cavity loss also depends nonlinearly with angle.

To overcome these problems an air-spaced etalon was used. An air-spaced etalon has the advantage of a constant tuning rate and a constant insertion loss which reduces the possibility of etalon mode hops. The latter is especially important since PPLN has a small residual absorption at 3μm. Thus, as the intracavity power changes due to rotation of the etalon, the temperature of the PPLN crystal changes slightly, which can induce tuning of the output wavelength. The etalon used in our system was composed of two wedged fused silica substrates spaced approximately 1mm apart which were AR coated on one side and uncoated on the other. This yielded a reflectivity of approximately 5%. A piezoelectric element was used to tune the etalon. An example of the scanning characteristics with the air-spaced etalon is shown in figure 5.

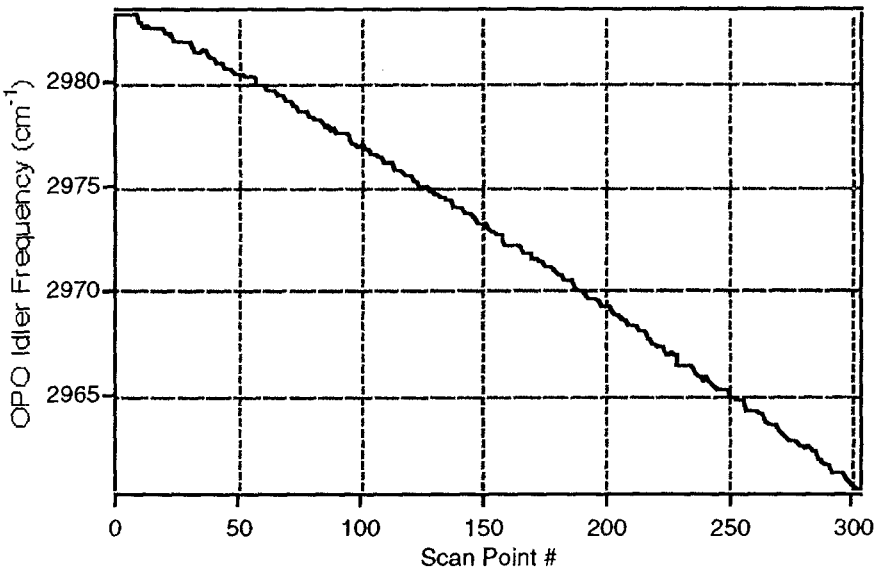

Figure 5. Mode-hop scan over 20 cm^{-1} obtained with a scanning air-spaced etalon and synchronous tuning of the PPLN crystal.

Continuous tuning

For continuous tuning it was necessary to tune the OPO cavity mode synchronously with the etalon. Our goal was to demonstrate approximately 1-2 cm^{-1} of continuous tuning using this approach. Figure 6 shows the cavity configuration used for continuous tuning. Here, an air spaced etalon was used to confine the cavity mode or oscillation frequency. An air-spaced etalon has the advantage in that it is tuned by varying the spacing of the air gap and not by rotating, thus eliminating the variable walk-

off losses. To achieve continuous tuning, the cavity length is varied either with an internal element such as a rotating Brewster plate or more simply by translating a cavity mirror. We have chosen the latter. This eliminates the need for inserting a lossy internal cavity element and also is somewhat simpler. The drawback is that large translations on the order of 40 μm are required. The most reliable method of translation on this scale is through the use of piezo-electric transducers. The cavity used in our setup used a multiple stack piezo which was capable of translations on the order of 40 μm. The effective tuning was actually twice this since the optical cavity length changes by twice the translation amount. The goal was to demonstrate approximately 1-2 cm^{-1} of continuous tuning.

As the cavity length is changed, i.e. shortened, the cavity modes shift to shorter wavelengths. The etalon is then slaved by a lock-loop to the peak of a cavity mode and tracks the cavity mode as the cavity is tuned. The challenge is to keep the etalon locked to the cavity mode as the cavity length is tuned. There are many perturbations which can disrupt the tuning process such as air currents inside the cavity caused by the PPLN oven. Rapid thermal changes in the PPLN crystal can change the effective optical length of the cavity. Some of the perturbations such as convection currents generated by the PPLN oven can be controlled by isolating the oven. Others, like the rapid thermal fluctuations inside the PPLN (caused in part by absoprtion of 3μm light in the crystal) crystal cannot be controlled. If the perturbations occur too rapidly, i.e., outside the bandwidth of the lock loop or if the perturbation was too large then the OPO would mode hop. To keep the insertion losses low the etalon was of relatively low finesse making the cavity more susceptible to mode hops. The etalon also had to be of low mass so that the loop response frequency would be high.

While the continuous tuning method described here has been used quite successfully on tunable dye lasers[7] the application to tunable OPOs possess many different challenges. In particular, we have observed that although the cavity mirrors are designed to transmit the 3.0 μm light there is enough feedback to cause a double resonance effect. Doubly resonant OPOs are in general very unstable. As the cavity length was tuned in our system the 1.5 μm light would tune continuously whereas the 3.0 μm light would tune continuously in the opposite direction. However, there were occasions when the 3.0 μm light was slightly resonant in the cavity which raised the intra-cavity 3 μm power. This in turn raised the temperature of the PPLN crystal which effectively changed the optical length causing the laser to tune uncontrollably. To mitigate this problem, we have purchased optics which were more effective in rejecting intra-cavity 3.0 μm light. Unfortunately, the intra-cavity etalon was somewhat lossy and

we have not fully tested this method of tuning with our OPO. We have however verified the performance of the etalon in another tunable OPO being developed at Coherent Laser Group in Santa Clara, CA. This system had the advantage of a higher pump power (10 watts) so the cavity could tolerate a higher intra-cavity loss.

As part of our commercialization goal and also to facilitate a more rapid development of the tunable laser source we have signed an MOU with Coherent Laser Group. As part of this collaboration we have obtained one of their tunable OPO's for evaluation. Coherent has a long history in the development of continuously tunable visible and near IR lasers and is also presently developing technology that would be useful for the tunable laser system being developed under SERDP support. Under the terms of the MOU, Sandia has acquired key lock loop and scanning technology. In addition, we will acquire broad band optics which should extend the broad tuning range of the laser. The lock loop technology developed at Coherent has already been tested with our air-spaced etalon and they have demonstrated over 2 cm^{-1} of continuous tuning with this system. Coherent has expressed great interest in manufacturing both the laser and also the sensor. We hope that following the MOU a CRADA would be put in place to continue development of the sensor.

The use of this system has been very valuable for evaluating different air-spaced etalons and lock loop technology. Since this OPO was pumped by a 9 watt IR VERDI laser (the SERDP system has 6 watts) higher intracavity losses could be tolerated. We have found that with a 20% reflectivity etalon and a spacing of approximately 1mm truly continuous tuning over a 1.5 cm^{-1} range could be obtained. Scanning in this cavity was achieved by rotating an intracavity Brewster plate which adiabatically changed the cavity length (and hence the frequency) and synchronously scanning the intracavity etalon. A lock loop, developed by Coherent was used to keep the etalon passband centered on the OPO cavity mode. Figure 6 illustrates a 1.5 cm^{-1} scan obtained by this method. The marker fringes were obtained by directing the 1.5μm light from the OPO into a fixed etalon and recording the transmitted light as the OPO was scanned.

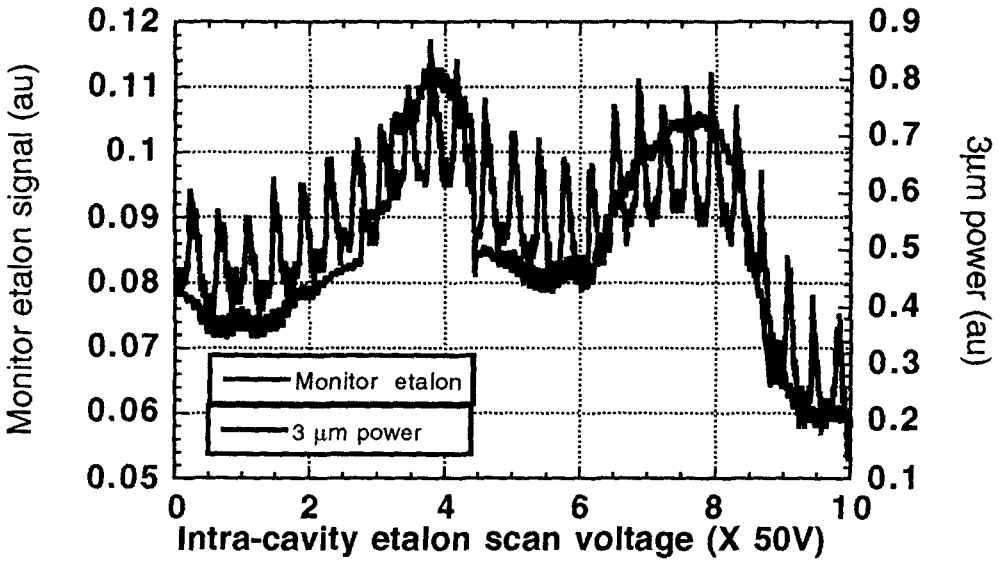

Figure 6. Continuous scan of the Coherent OPO. The monitor etalon marker fringes show that the scan was truly continuous with a scan range of approximately 1.5 cm^{-1}. The apparent modulation in the 3μm power is not yet understood but it is suspected that spatial mode profile changes coupled with the use of a small area detector may produce this effect.

A possibly improved method of tuning would be to translate the cavity mirror over a long range (i.e. 40μm) and remove the Brewster plate. The Brewster plate increases the intracavity losses but also modulates the intra-cavity power which is undesirable. This method of tuning is currently being investigated in our laboratory.

Photoacoustic Spectroscopy

Background

The wide range of physical properties of the gaseous pollutants defined under the Clean Air Act Amendment poses a formidable detection challenge. Photoacoustic spectroscopy is an ideal method of detection since it is sensitive and capable of detecting species with both broad and narrow spectral features. Photoacoustic spectroscopy operates by monitoring the heat deposited in a volume containing the gas of interest while scanning the input wavelength. This is in contrast to traditional spectroscopic techniques which monitor the *transmitted* or absorbed laser light as a function of wavelength. Many absorption techniques such as frequency modulation and wavelength modulation

spectroscopy are derivative techniques and in general are sensitive only to small molecules with well defined spectral features (large derivatives) but are not amenable to large molecules with broad spectral features. The difference between the spectra of a large molecule such as toluene and a small molecule such as NO_2 are illustrated in figure 7. Only photoacoustic spectroscopy has all of the attributes required for a CEM monitor. Another advantage is that under normal operating conditions it is a linear technique thus facilitating easy analysis.

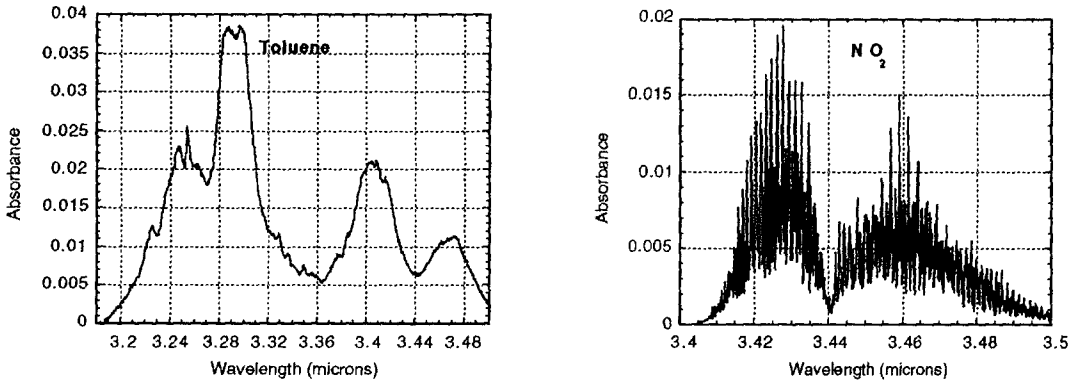

Figure 7. Comparison of absorption spectra for a large molecule such as toluene and a small molecule such as NO_2. Photoacoustic spectroscopy is ideal for the detection of species with both broad and narrow spectral features.

The heat deposited in photoacoustic spectroscopy is monitored not by the temperature but by the acoustic pressure wave that is created by the expanding hot gas. A simple hearing aid microphone is sufficient for this purpose. The technique can be employed in either pulsed or cw modes. In the pulsed mode, a pulsed laser is directed into a cell containing the gas to be monitored and the ballistic pressure pulse is then detected. For continuous wave (cw) operation, a cw laser beam is chopped (usually at a few KHz) and the chopped acoustic frequency is detected, not individual pulses. We have explored the pulsed mode of operation in our laboratory and found that while pulsed operation was sensitive the PPLN laser technology was actually more mature for cw operation. Therefore, this is the path that we have chosen. CW operation does however place some difficult requirements on the laser. In general, to achieve high sensitivity it is desirable to have an average power of a watt or greater. High intensity on the other hand is undesirable as the spectral resolution can be degraded. These seemingly mutually

exclusive requirements can be met through the use of an acoustically resonant cell. Here the acoustic signal is resonantly enhanced by using an acoustically resonant cell. This simultaneously reduces the required excitation power and also reduces the potential for spectral power broadening.

Cell Design

There are several criteria that need to be considered in the design of a photoacoustic cell for a field portable sensor. For cw operation the cell should be acoustically resonant to enhance sensitivity and the windows should be isolated from the main resonant chamber. Furthermore, for rapid analysis the volume should be small so that the gas volume can be exchanged rapidly. A large mass is also desirable to dampen external acoustic noise. The strength of the photoacoustic signal depends on a number of factors: the overlap of the laser beam and the acoustic mode being excited, the intensity of the laser beam, the excitation or chopping frequency, the volume and Q of the cell and the absorption properties of the gas.

Figure 8 illustrates one of the resonant acoustic cell designs we have tested. In this design a chopped cw laser beam entered the cell through an acoustic filter and then into the main acoustic chamber. The acoustic filters were used to reduce window noise (due to absorption of the laser beam) from reaching the microphone. Furthermore, the main acoustic chamber is mounted at an angle to the laser beam. This is so that the laser beam would be coupled into the cell at a node of the acoustic cell thus further reducing the potential for the coupling of outside noise into the microphone. This idea was first demonstrated by Gerlach and Amer[8] and is the basis for the approach used here. The cell design in figure 6 is a variant of this design and was developed by Meyer and Sigrist.[9]

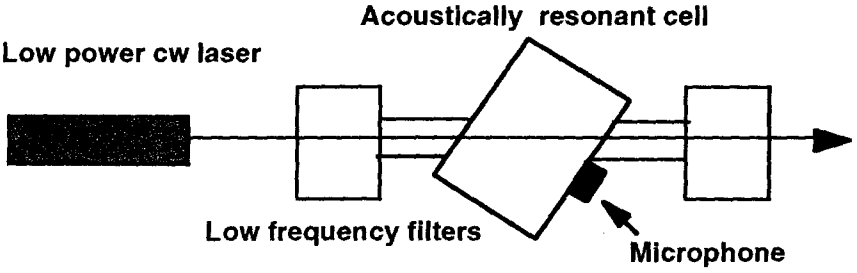

Figure 8. Design for an acoustically resonant cell. The filters at the input and output of the cell are used to reduce the coupling of window noise into the main acoustic chamber. The main acoustic chamber is mounted at an angle with respect to the main beam and at an acoustic node to reduce coupling of noise.

This cell has a resonant frequency of 2675 Hz and a Q of approximately 200. The main resonant chamber is circular with dimensions of 6.54 cm × 15.56 cm (diameter) yielding a volume of 1243 cm^3 . We have found that while the cell had a high Q and was therefore quite sensitive it was prone to picking up background noise. The background noise had three main components: a random component, a coherent component proportional to the laser power and a coherent component that was independent of laser power. The main source of noise was coherent noise generated from the chopper wheel. This noise has been reduced by evacuating the air inside the chopper wheel. We have also found that evacuation of the cell was extremely difficult. Since the cell could not be pumped down as this would damage the microphone diaphragm, it was necessary to purge the cell for several minutes with pure nitrogen. Even with purging, the large volume of the cell coupled with the residual pockets of gas made the cell extremely difficult to refill. This made the cell impractical for field use.

Under a collaboration with Dr. Jos Oomens of the Catholic University of Nijmegen, The Netherlands, we have experimented with an alternate acoustic cell design. A schematic of the cell is shown in figure 9. While this design was similar to our original design in that it had a main acoustic chamber and acoustic traps to reduce window noise there were some very important differences. The volume of this cell was considerably smaller (15 cm × 1.78 mm diameter) which allowed for rapid exchange of gas. Moreover, since the acoustic excitation amplitude is inversely proportional to the volume the excitation amplitude was considerably greater. The excitation amplitude is also inversely proportional to the resonant frequency squared and for this cell the resonant frequency was approximately 1600 Hz, which was considerably lower than the resonant frequency of our first cell (2675 Hz). Finally, the cell was much more massive which greatly reduced the coupling of external acoustic noise into the cell. Thus, even though the Q of this cell was much lower than our original design the combination of a larger mass, smaller volume and a lower resonant frequency made for a more sensitive cell. This cell was extremely sensitive and has even been used to detect the respiration of cockroach and even a gnat.[10,11] The lower Q (~10) of this cell is also desirable in a field environment since the cell temperature can change thus shifting the cell resonant frequency and response.

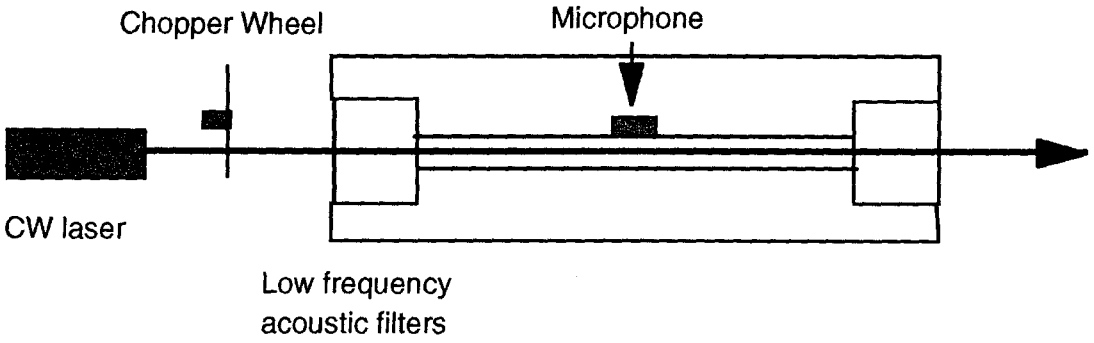

Figure 9. New photoacoustic cell design. The smaller volume and lower resonant frequency combined to give high sensitivity while the small volume allowed for rapid gas exchange.

Using this cell with the PPLN laser source we have made sensitivity measurements of ethane and pentane. These measurements were made with the gas diluted in pure nitrogen and at atmospheric pressure. These data are shown in figure 10. For ethane, we achieved an extrapolated sensitivity of approximately 15 ppb and for pentane the extrapolated sensitivity was approximately 22 ppb.

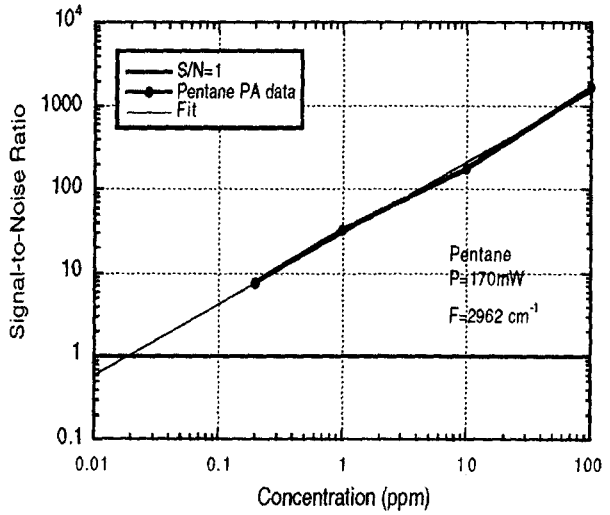

Figure 10. Photoacoustic sensitivity measurement of pentane.

The windows of the cell were ZnSe, tilted at Brewsters angle to reduce reflection losses and to avoid stray reflections which could raise the acoustic background level. Although

the Q of this cell was very low compared with the previous design, the combination of low cell volume and low resonant frequency yielded a responsivity that was nearly equivalent.

Cell Calibration

To obtain an interpretable photoacoustic spectrum the photoacoustic signal must first be normalized to the input signal, otherwise the resultant spectra will be intensity dependent. Normalization is accomplished by picking off a small fraction (i.e. 1-5%) of the incident beam and then ratioing this with the photoacoustic signal (figure 11). In principle, normalization will compensate for intensity fluctuations but other effects such as detector nonlinearity, detector window etaloning, detector homogeneity, and beam profile changes all can cause residual noise. We have found the largest source of noise were beam profile changes associated with both intensity and frequency fluctuations. To eliminate this source of noise a lens was inserted into the reference beam path to focus the light tightly onto the face of the reference detector. The reference detector was a Molectron pyrometer with a detector area of approximately 5mm. This type of detector has several advantages over semiconductor types in that the spectral response is much flatter and that there are no windows to cause etaloning.

Having calibrated the reference detector it was then necessary to determine the cell responsivity, R (μVolts / (C*mW*α) where α is the absorption (1 / ppm-m) and C is the concentration in ppm. If the cell is operated at a pressure other than at atmospheric pressure then absolute units (1 / (N^3-m)) should be used for concentration. Gases with known absorptions (α's) and concentrations were then used to determine the cell responsivity. Under atmospheric conditions the calibration should be independent of the calibration gas since energy transfer from vibration/rotation to translation (heat) is nearly 100%. We have used several gases for calibration: methyl ethyl ketone, isopropyl acetate, n-butyl acetate and butane. Calibration constants varied from 103 (butane) to over 300 μV-m/mW. There were several reasons for the wide variations; some of the VOC's were slightly polar and therefore stuck to the surfaces of the gas bottle and photoacoustic cell, thus lowering the effective concentration, and second, the absorptions of some of the VOC's were not known accurately. For butane however, which is a nonpolar species, the calculated cell responsivity was from 150 - 200 μV-m/mW at high concentrations (>50ppm) but at low concentrations (5 ppm) was reduced to approximately 80. The source of this discrepancy has not yet been determined but we have found variations as large as 20% in the gas dilution system.

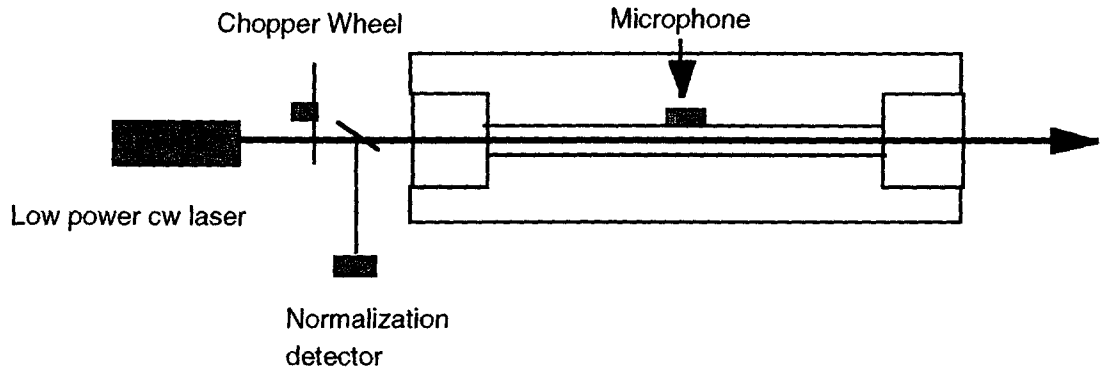

Figure 11. Since photoacoustic spectroscopy is an intensity dependent technique, a reference detector must be used to normalize the photoacoustic signal.

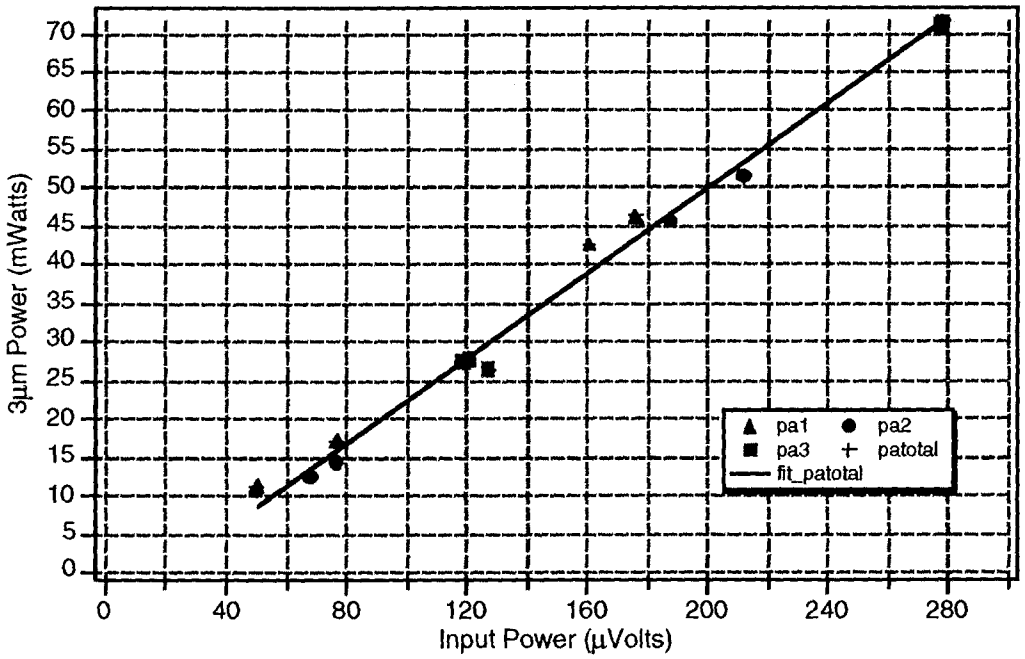

Figure 12. Calibration of the reference detector, illustrating linearity, offset and fit precision.

In this work we have used a intermediate value of 200μV-m/mW for the cell responsivity. This was for a two pass configuration and would obviously change with the number of passes. It might then seem desirable to increase the number of passes through the photoacoustic cell but it has been determined experimentally that two passes were optimum. There were two reasons for this. First, the window noise increases with each pass and second, with more than two passes an off axis beam geometry must be used. This, coupled with beam profile changes that were observed with etalon mode hops,

produced quite a noticeable modulation in the photoacoustic signal when more than two passes were used.

Spectrometer

Figure 13 shows a photograph of the photoacoustic system. The major components of this system are the pump laser (VERDI manufactured by Coherent Inc) the PPLN OPO, the photoacoustic cell and the data acquisition, control and analysis computer (IBM Think Pad). The components were mounted on an optical breadboard

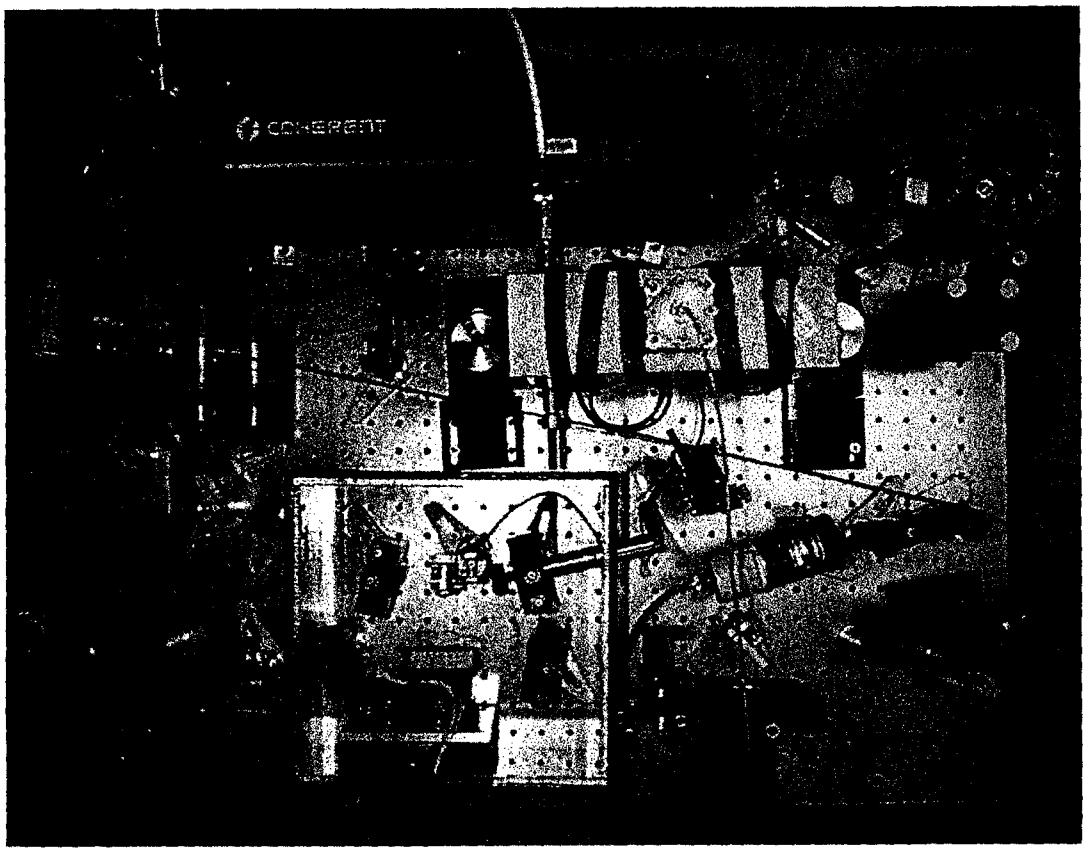

Figure 13. Photograph of the photoacoustic spectrometer showing major components such as the pump laser (top), photoacoustic cell (center) and the PPLN OPO at the bottom.

approximately 3 ft by 2 ft which permitted easy access to hardware and also easy modification. The system is stand alone except for the requirement of 120V 15A electrical service. No cooling water was required for the laser. All data acquisition, control and analysis were near real-time thus eliminating the need for post analysis.

Although not shown in figure 13, a Burleigh wavemeter was used to record the 3 μm light from the OPO. Ultimately, we hope to replace the wavemeter with a molecular calibration cell to obtain absolute wavelength measurements. Also not shown in the photograph were two lock-in amplifiers which were used to detect the microphone signal and to detect a fraction of the 3 μm light for normalization (ratioing) with the photoacoustic signal. It was necessary to ratio the photoacoustic signal with the normalization measurement since the OPO power could change while scanning. The analog output of the lock-in amplifiers were then fed directly into the computer.

All of the data analysis, acquisition and control was performed by LABView software running on a laptop computer. The interface between the computer, laser and photoacoustic cell was through a PC-MCIA card and a GPIB card installed inside the IBM laptop. These cards were about the size of a credit card and were extremely versatile as they had many input and output channels. At this point, most of the laser scanning control and data acquisition has been automated. The scanning etalon and PPLN stepper motor were controlled through the PC-MCIA card and the wavemeter was controlled through a GPIB interface.

System Characterization

The requirement for quantitative measurements of gas mixtures, comprised of both narrow line and broad absorbers, requires careful characterization of the system. The system sensitivity, linearity and selectivity to both broad and narrow line absorbers all must be determined. In addition, different averaging and scanning modes must also be evaluated. The mode of operation will ultimately depend upon the measurement conditions such as effluent concentrations and interfering species such as water vapor.

For narrow line absorbers it was necessary to scan the laser very precisely over the spectral line. Methane was used for this since its lines are narrow. Figure 14 shows an example of a doublet line of methane acquired with mode-hop tuning of the system. This agrees well with the theoretical HITRAN spectrum. Even though the mode hops were on the order of 600 MHz (.02 cm^{-1}) the spectral features were well resolved. The next task was to evaluate high resolution scanning over a broader spectral range. This was accomplished by simultaneously scanning the PPLN crystal with the etalon and is shown in figure 15 for the Q-branch of methane. For comparison, a theoretical Q-branch spectrum from HITRAN is shown which is in excellent agreement. This spectra was acquired with the older, larger photoacoustic cell and was normalized using a $1mm^2$ area lead selenide detector.

For species with broad absorption features (i.e. many VOC's) it was not necessary to scan the laser. Instead, spectra could be acquired at a few discrete wavelengths, chosen so as to be free from water vapor and methane interferences. This mode of acquisition had the advantage over scanning in that the signal to noise ratio could be enhanced significantly. In fact, this is the mode of operation that was used in the field, at least in situations where species with broad spectral features were to be detected. Figure 16 contrasts the signals for isopropyl acetate with both discrete and mode hop tuning. Clearly, for high sensitivity, it is desirable to average at discrete wavelengths. This is also illustrated in figure 17 which shows a 16 point butane scan at a concentration of 5 ppm.

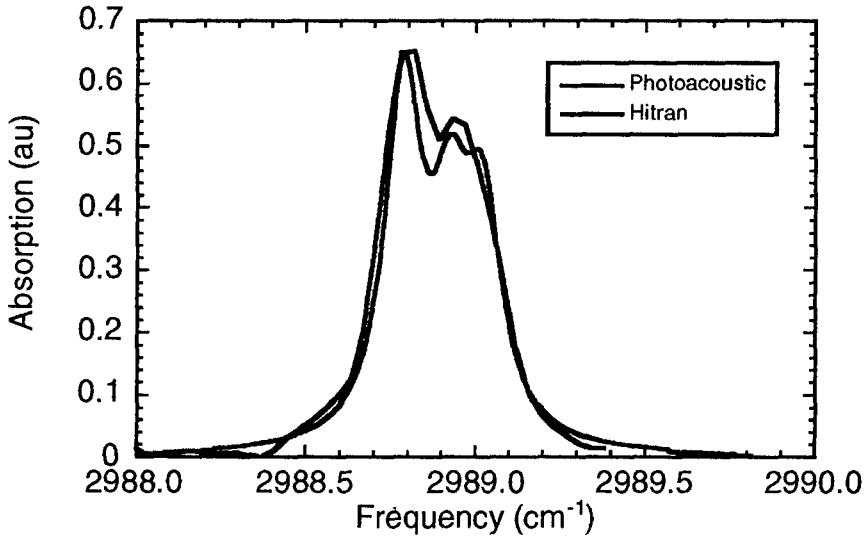

Figure 14. Photoacoustic scan over a double line of methane, illustrating spectral resolution.

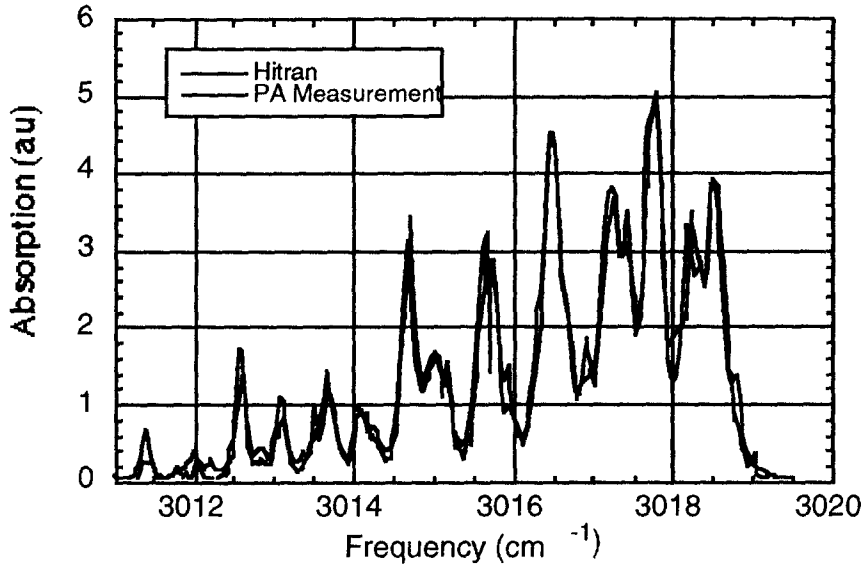

Figure 15. Q-branch of methane taken with this cell using the mode-hop tuned PPLN source.

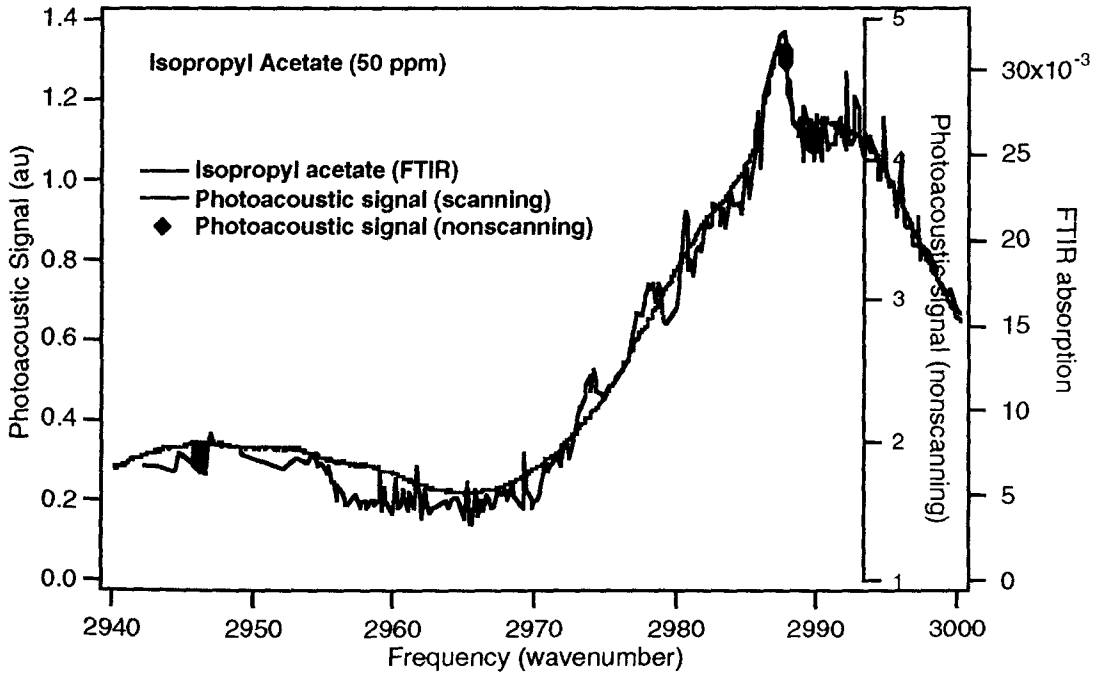

Figure 16. Measurements of isopropyl acetate at 50ppm acquired under scanning conditions (red) and discrete frequencies (magenta). The advantage of using discrete frequencies is that signal averaging can be increased, thus enhancing the sensitivity.

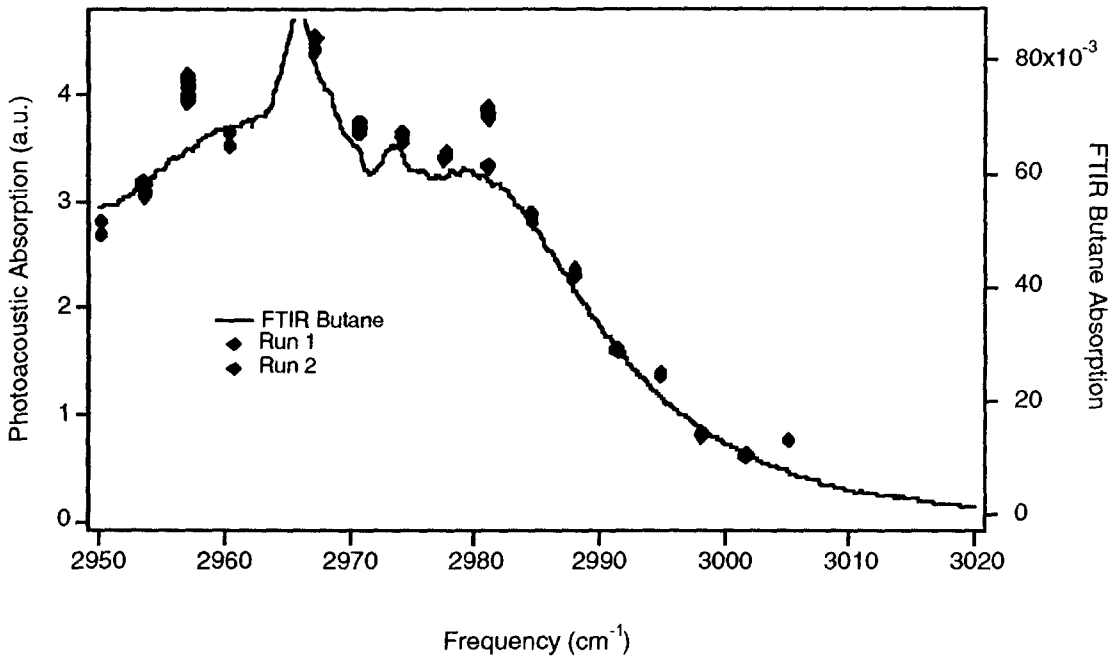

Figure 17. Photoacoustic spectrum of butane acquired at a concentration of 5ppm. The large offsets near 2960 and 2980 cm^{-1} are caused by fortuitous coincidences with water vapor.

Field Test

Issues

The detection of trace volatile organics in an application such as compliance monitoring is a challenging problem for many reasons. First, many organics of interest have broad, somewhat featureless, overlapping spectra which makes speciation difficult. Furthermore, concentrations are typically low (in the high ppb to low ppm range) while the concentration of potential interferents such as water vapor are relatively high (~ 5000ppm), which illustrates the measurement challenge. Fortunately, the water vapor windows are deep enough to allow measurement.. In addition, the absorption strengths are typically lower than that for water vapor. Finally, many of the organics considered here are somewhat sticky which can make sampling and measurements both difficult and inaccurate. The situation is illustrated in figure 18 which shows the spectra of methyl ethyl ketone, n-butyl acetate, isopropyl acetate and toluene. Clearly, speciation will require tuning over a broad spectral range although the tuning need not be continuous. The choice of wavelengths depends on both the number and type of species to be measured. In the cases considered here there are several key differentiating spectral features. For methyl ethyl ketone (MEK) and isopropyl acetate there are distinctive "Q"

branch like features near 2990 cm^{-1} and a weaker MEK feature near 2949 cm^{-1}. For the aromatics such as toluene, M, O and P xylenes etc.., there are absorptions at frequencies above 3020cm^{-1} which are well separated from the ketones and acetates. In general, aliphatic hydrocarbons have two C-H absorption bands: a strong band attributable to the terminal methyl groups ranging from approximately 2980-2960 cm^{-1} and a weaker band near 2970-2920 cm^{-1} attributable to backbone methylene groups. Aromatics can have absorptions in these same regions due to attached groups but in addition there is distinctive absorption band from 3060-3030 cm^{-1}. Figure 19 illustrates the absorption spectra of several components found in paints and solvents. The aromatic, methylene, and end methyl absorptions are evident.

In principle, only a few wavelengths are needed for speciation but the choice of wavelengths will depend on knowledge of the effluent stream and there are also restrictions due to absorption by water vapor. Figure 20 shows a simulated absorption spectra of a multi-component organic emission overlaid with the absorption spectra of water vapor. The water vapor spectrum is plotted on a log scale so as to illustrate the contribution of the water vapor continuum. Quite fortuitously, for the sensitivities required here, the water vapor continuum is weak enough so that it is not a factor.

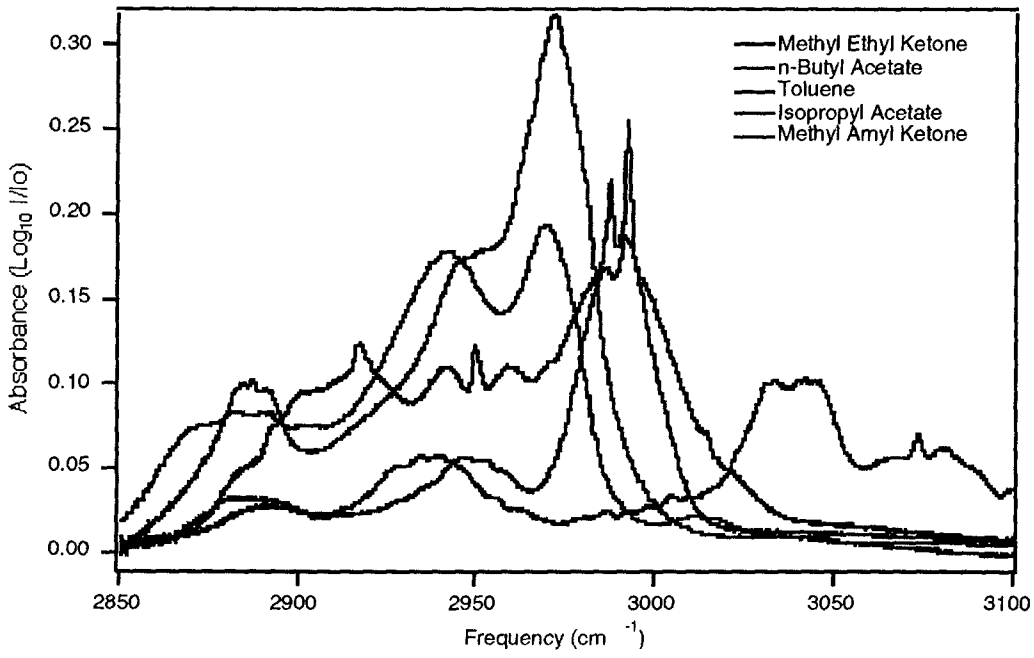

Figure 18. FTIR Absorption spectra of several volatile organics of interest which are found in paints.

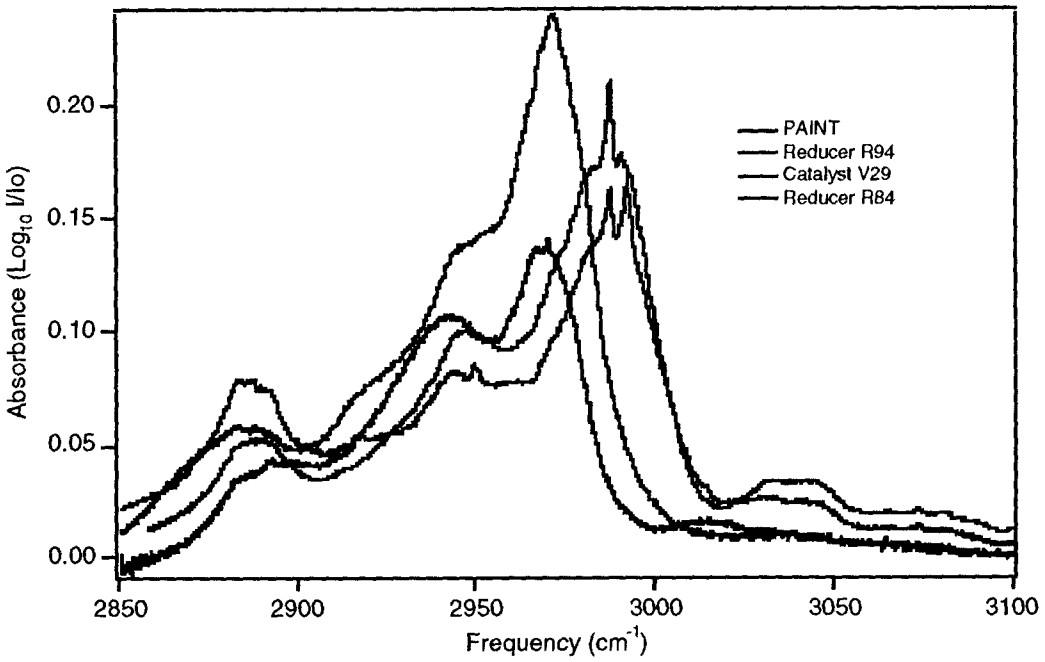

Figure 19. FTIR absorption spectra of volatiles from a typical paint catalyst, solvent and two reducers.

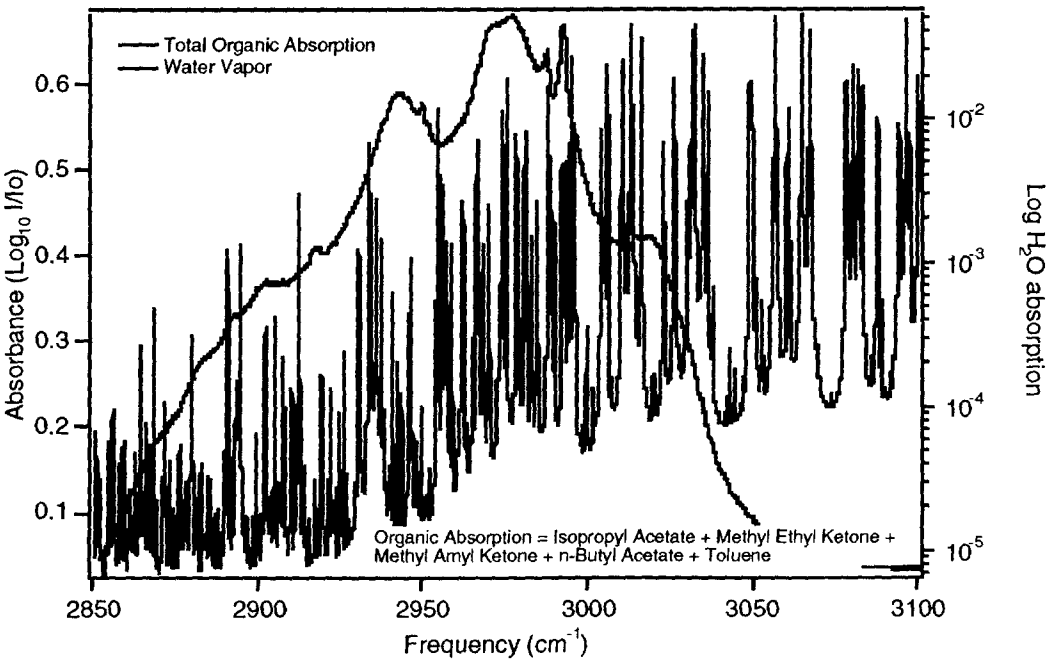

Figure 20. Absorption spectrum of a simulated organic emission composed of toluene, isopropyl acetate, n-butyl acetate, and methyl ethyl ketone (red curve) overlaid with water vapor. In actuality, the organic absorption would be much weaker than water vapor.

Field Demonstration

For our first field demonstration we have selected the painting facility at the Lawrence Livermore National Laboratory. This is an ideal facility for many reasons: painting facilities are high on the list of monitoring needs for the DoD and DOE, many of the effluents are defined as CAAA pollutants, a wide range of VOC's are emitted thus demonstrating the need for a broadly tunable photoacoustic spectrometer, and a water curtain is used to scrub effluents from the exhaust stream which will entrain water vapor, thus providing an opportunity to detect VOC's under difficult conditions. The water curtain will also simulate conditions that might be found in an incinerator. Many of the effluents associated with painting are also used in many other DoD processes such as munitions manufacturing and so will provide a benchmark of performance for other applications. Furthermore, our close proximity to LLNL will allow for extended testing. We have also contracted with the Chemistry and Enivronmental Protection departments for independent analysis of the effluents. A photo of the paint facility is shown below in figure 21. Painting is performed inside a room with a large negative air pressure which draws effluents through a water curtain and out of a stack. The main function of the water curtain is to trap particulates but it is also effective for the reduction of VOC emissions. We have determined from a GCMS analysis both before and after the water curtain that approximately 60-70% of the VOC emissions makes it through the water curtain. Typical concentrations are in the low ppm range. Our focus will be on the detection of VOC's emitted from oil based paints. Specifically, we are examining Polane brand paints which consist of three components: reducer, catalyst and paint. For the reducer, the major components are: methyl ethyl ketone (2-butanone or MEK), isopropyl acetate, n-butyl acetate and toluene. The catalyst has many components (primarily isocyanates which are polymerizing agents) but only n-butyl acetate and methyl amyl ketone (MAK) are volatile. The paint has pigments such as TiO_2 and volatiles such as MEK, MAK, methyl isobutyl ketone (MIBK) and isopropyl acetate. A typical mixture of paint, catalyst and reducer is 4 parts paint to 1 part catalyst diluted with 25% (of total volume) or more reducer.

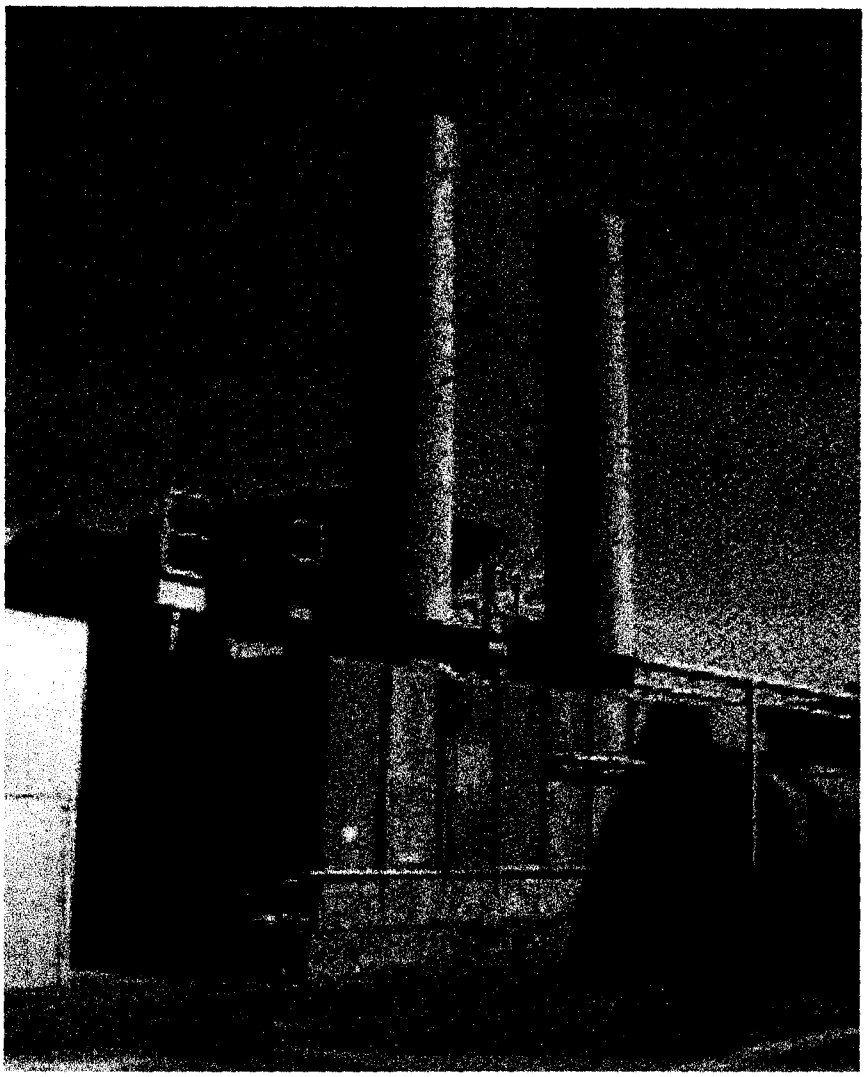

Figure 21. Photograph of the LLNL paint shop stacks. Effluent is pulled from the paint booth through a water curtain and out the stack. The sampling probe was installed just below the exhaust fan (at the base of the stack).

Gas sampling was performed via a 50 ft PFA type 3/4" teflon line which was resistant to sticking by VOC's. A small pump was then used to *draw* air in from the stack through the sample line up to the photoacoustic cell. This configuration avoided the problem of pump oil from entering the cell. After filling the sample line, the pump was then reconfigured by a gas manifold so that gas could be drawn from the sample line through the photoacoustic cell. By using a low flow rate through the cell the microphone could be protected from large pressure transients. Also attached to the gas manifold is a port for a GCMS sampling bottle. Typical sample volumes were on the order of several

liters. Post analysis was immediately performed to avoid sample degradation (i.e. sticking). Unfortunately, GCMS analysis was not availbale during actual field tests. All sampling during the field test was performed after the water curtain. Table 2 below summarizes effluents for a typical measurement both before and after the water curtain. Although not reported here, the water vapor concentrations were around 5-10 parts per thousand and so were quite large compared to VOC concentration. Water vapor concentrations were determined by a Vaisala Humidicap sensor.

Table 1. Components of several paints used at the LLNL paint shop.
V- Volatile, NV- non Volatile.

Paint **POLANE High Solids Plus**	**TiO_2** **Methyl ethyl ketone (V)** **Methyl amyl ketone (V)** **Isopropyl acetate (V)**
Reducer R84	**Isopropyl acetate (V)** **Toluene (V)** **N-butyl acetate (V)**
Reducer R94	**Toluene (V)** **Isopropyl acetate (V)** **n-butyl acetate (V)**
Catalyst V66V27	**Toluene diisocyanate polymer (NV)** **1-methoxy 2propianol (NV)** **Toluene 2,4 Diisocyantes (NV)**
Catalyst V66V29	**Hexamethalene diisocyanate biuret (NV)** **n-Butyl acetate (V)** **Hexamethylene diisocyanate (NV)**

Table 2. Compounds measured by GCMS before and after water curtain.

Compound	Water Curtain (conc. ppm)	Inside (concentration ppm)
2-Butanone (MEK)	6.5	6.8
Isopropyl Acetate	2.7	2.8
Toluene	2.7	2.7
n-Butyl Acetate	2.4	2.7
2-Heptanone (MAK)	1.3	1.4

Field Measurements

We have now completed our first field test and have successfully demonstrated the ability to detect, speciate and quantify VOC's at low concentrations while in the presence of water vapor. The primary objectives of the test were to quantify and speciate a mixture (i.e. 4-5 species) of spectroscopically similar VOC's at ppm level concentrations and determine the effect of the water vapor continuum on the sensitivity. Measurements were acquired under a variety of conditions, i.e. relative humidity, wavelength, paint type and concentration. We have also examined the retention of VOC's in the water curtain bath as this was also source of VOC emission, even after several hours. All measurements were acquired with the water curtain both during and after painting operations. Background measurements were made early in the morning before painting operations. Data were analyzed using both a simple best fit and also using a full chemometrics code developed under another program. A summary of the paints measured and their volatile components is given below in table 3. Paints are group according to the catalyst, reducer and paint mixture.

In a typical measurement, data were acquired at approximately nine wavelengths which were chosen on the basis of absorption strength and also to pick out features specific to a given species. There was also the requirement that the wavelengths be free from water vapor interferences. In general, wavelengths near 2950 cm^{-1} could be used to identify the presence or absence of MAK, 2970 cm^{-1} for n-BAC, and wavelengths near 3040 cm^{-1} are useful for aromatics such as toluene. Above 3000 cm^{-1} the absorption due to water vapor is significant and even between water vapor lines some absorption can be seen. For IPA and MEK, which both have distinguishing peaks near 2990 cm^{-1} (figure 18) , the situation is made difficult by strong water vapor interferences. In this case, the sides of the absorption bands near 3000 cm^{-1} can be used for identification from other

species but then it is not possible to isolate MEK from IPA. The use of more frequencies may help here, but a water vapor scrubber is another possibility.

Figures 22 through 28 show selected data acquired for a variety of different types of paint, reducer and catalyst. Each point is an average of 100 measurements taken 25 times for each wavelength. The fits were determined using data from the Hanst data base and also from in-house FTIR measurements. Although all of the data in these figures were acquired during painting operations there were significant differences in the measured concentrations. The most likely causes were the position, orientation and adjustment of the spray gun. We have also seen that the water curtain bath retains approximately 20% of the VOC's for several hours. Background water curtain measurements were also made in the morning before painting operations and VOC concentrations were below detectability limits (100's of ppb). A summary of selected measurements with their resultant concentrations are given in table 4.

Apart from the signal strength, the other major differentiating features of these data were the presence or absence of certain distinctive spectral features. The MAK absorption feature near 2950 cm^{-1} is clearly visible in all of the data, except in figure 25 which used the V66V55 catalyst and the RCK30 reducer. This was consistent with the known composition. In most cases, toluene was the only aromatic and hence was easy to identify. Since toluene absorbs above 3000 cm^{-1} where the water vapor absorption is dense, care had to be taken to avoid interferences. In figures 22, 25 and 26 some interference due to water vapor absorption on the wings of a line was observed. This was later corrected by moving the laser wavelength slightly. It is interesting to note that the data from March 8 (figure 27) clearly show the presence of toluene, whereas data from March 9, which used the same mix of paint from the day before, showed no evidence of toluene, suggesting either evaporation or reaction.

The only other aromatics were xylenes which were used in the V66VB11 accelerator and Polane High Solids paint. These were not observed in the signal which may have been due to masking by toluene, which has a higher vapor pressure and also occurred in higher concentrations in the mixed paint. Furthermore, xylenes have low vapor pressure and may also be scrubbed by the water curtain more effectively.

Some species were easy to identify by themselves but when in a mixture speciation became difficult. An example is provided by isopropyl acetate and methyl ethyl ketone which as explained above have several distinguishing features which are masked by water vapor. We identified the presence of these species from the stronger methylene absorption near 3000cm^{-1}. However, speciation was difficult and errors on the order of 50% or more are possible. Clearly, more wavelengths are needed for speciation.

The use of a water scrubber could also be of help here. In addition to MEK and IPA MIBK and n-BAC were also difficult to speciate.

Table 3. Volatile components of the 4 paints measured grouped according to mixture.

Paint Mixture	MIBK	MEK	MAK	IPA	n-BAC	Tol.	Xyl.
Polane Enamel	X		X			X	
V66V27 Catalyst							
R94 Reducer			X	X	X	X	
Polane Enamel	X		X			X	
V66V29 Catalyst					X		
R94 Reducer			X	X	X	X	
Polane Enamel	X		X			X	
V66V44 Catalyst			X				
R94 Reducer			X	X	X	X	
Polane High Solids		X		X	X	X	X
V66V55 Catalyst					X		
RCK 30 Reducer			X				
V66VB11 Accelerator	X						X

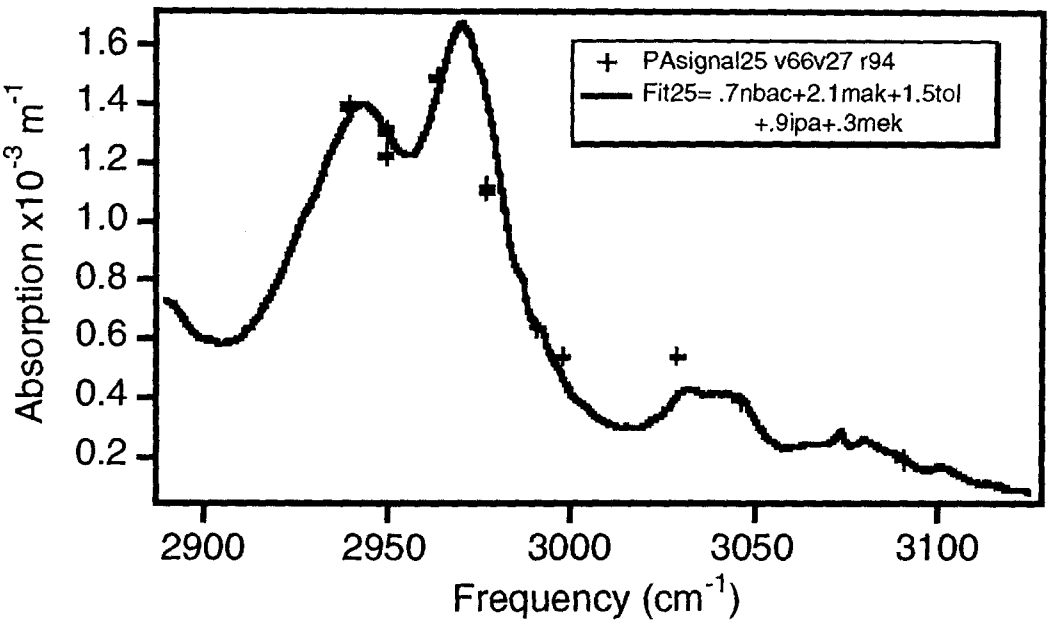

Figure 22. Measurement of a paint mixture with MAK component. The aromatic component (toluene), while weak by comparison, is easily isolated from the absorption of MAK, n-BAC and IPA.

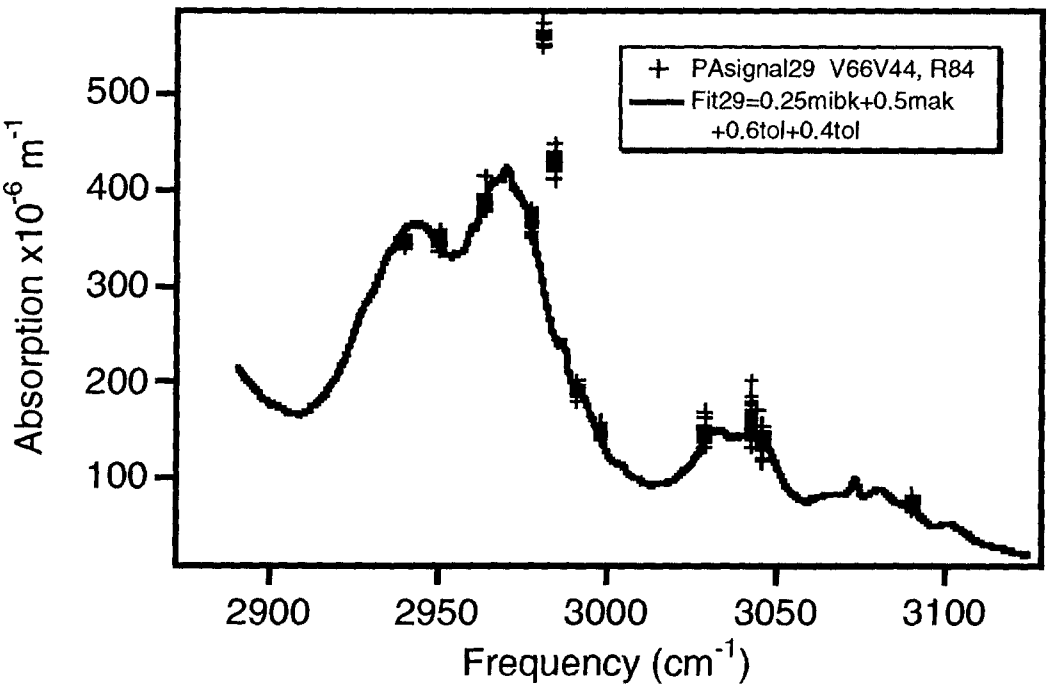

Figure 23. Measurement of a paint mixture with MAK, methyl isobutyl ketone, isopropyl acetate and toluene. The large differences near 2990cm^{-1} and 3050cm^{-1} were due to water vapor interferences. The equivalent absorption ($\Delta I/I$)was approximately 4×10^{-5}.

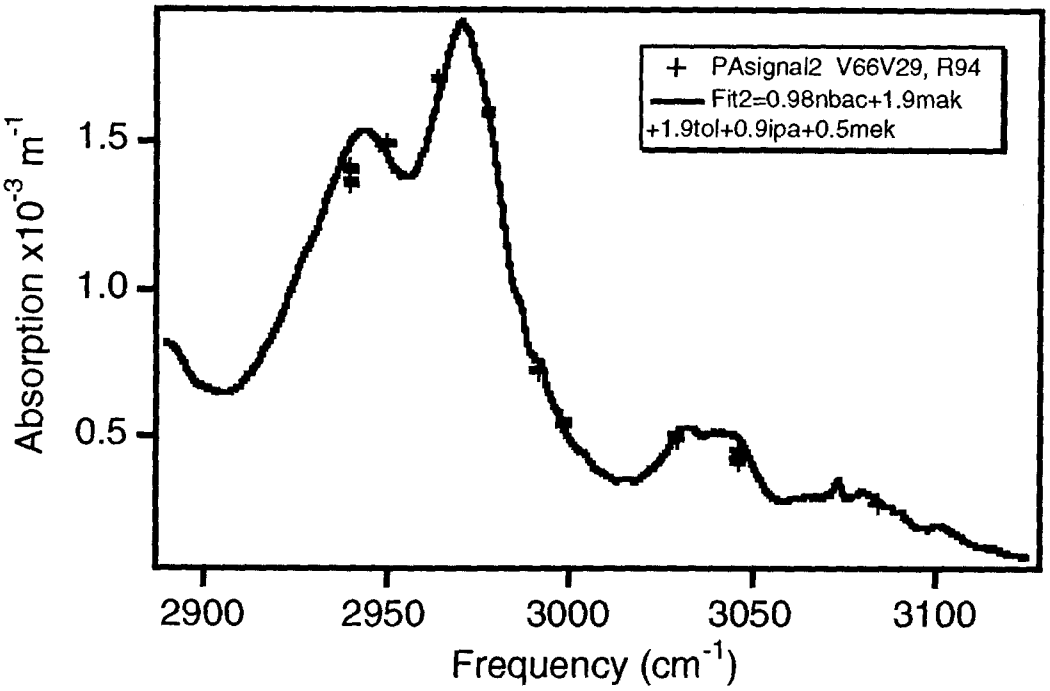

Figure 24. Measurement of a paint mixture with MAK component. The aromatic component, while weak by comparison, is easily isolated from the absorption of MAK, n-BAC and IPA.

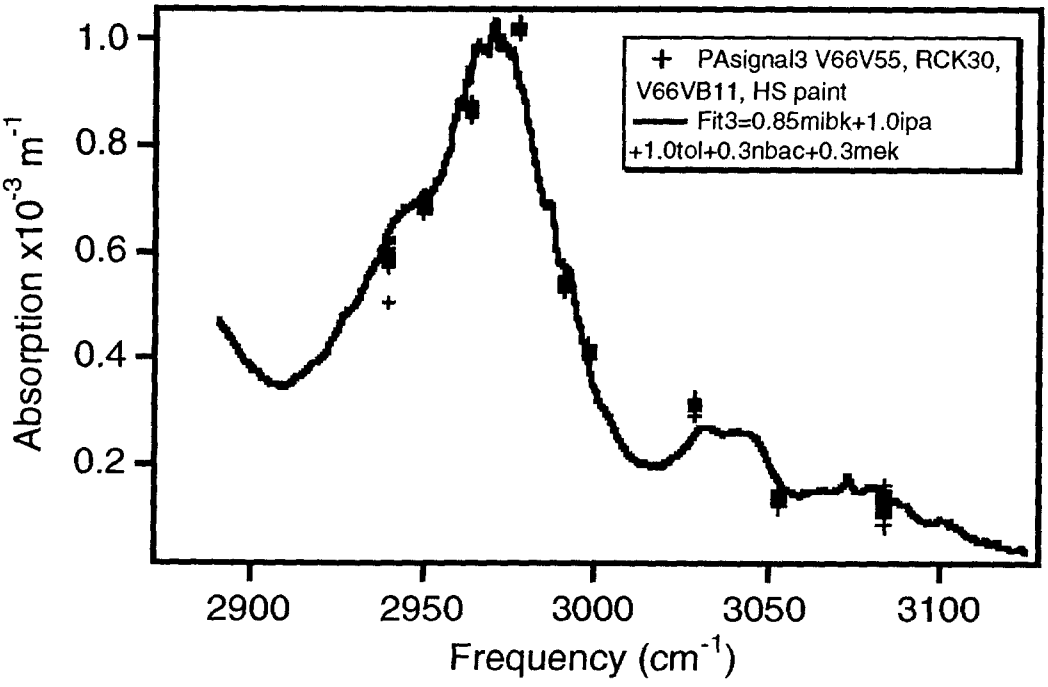

Figure 25. Paint mixture without the MAK component.

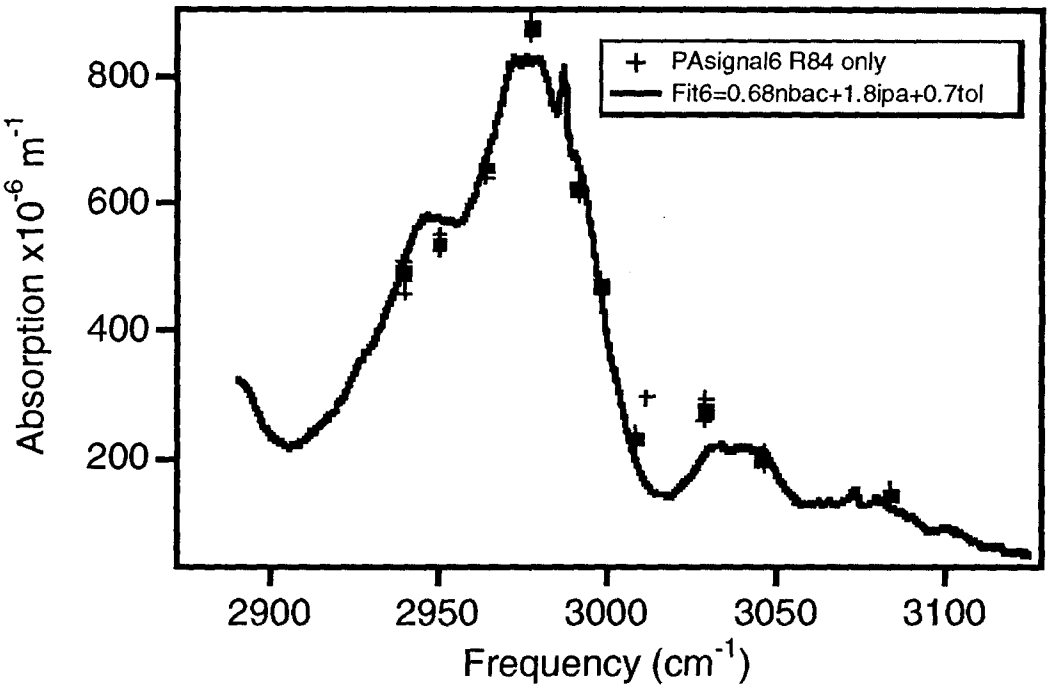

Figure 26. Measurement of reducer R84 without paint. MAK is clearly absent from this measurement.

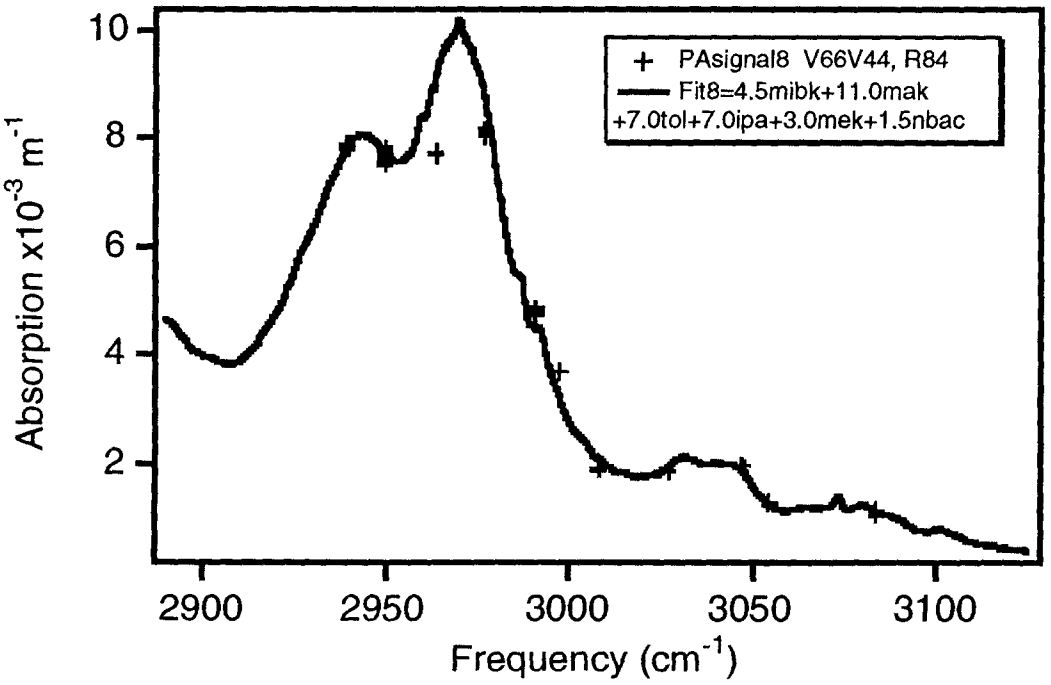

Figure 27. Measurement of a paint mixture with reducer R84.

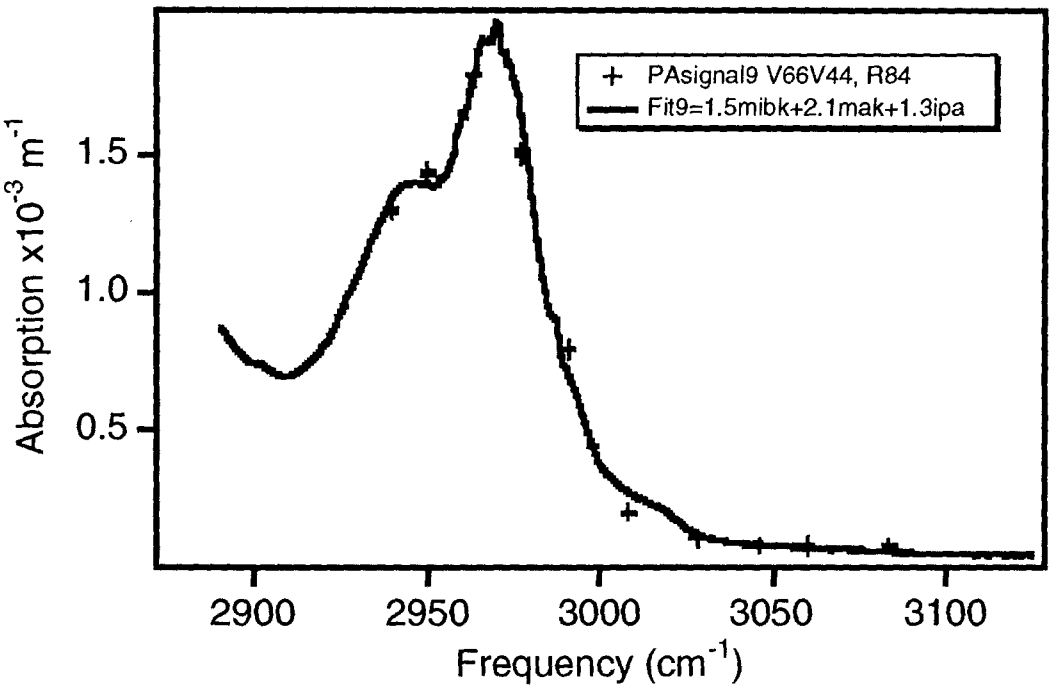

Figure 28. This paint mixture was the same as was used on March 8 (figure 27) but was stored for a day. Note the absence of toluene.

Table 4. Measured concentrations for selected runs.

	Concentration (ppm)						
Date	MIBK	MEK	MAK	IPA	n-BAC	Tol.	Xyl.
2/25/00	0.0	0.3	2.1	0.9	0.7	1.5	0.0
2/29/00	0.25	0.0	0.5	0.9	0.0	0.6	0.0
3/2/00	0.0	0.5	1.9	0.4	0.9	1.9	0.0
3/3/00	0.85	0.3	0.0	1.0	0.3	1.0	0.0
3/6/00	0.0	0.0	0.0	1.8	0.68	0.7	0.0
3/8/00	4.5	3.0	11.0	7.0	1.5	7.0	0.0

Error Analysis

The uncertainties of the above measurements can be divided into two categories: absolute error which is determined by cell calibration, uncertainties in published absorption data, and relative error, which is determined by statistical noise and fit precision. It should also be noted that all measurements were acquired with a static cell (the cell is filled, then closed off) thus the variability of the effluents cannot be resolved on short time scales, i.e. 10 minutes or less.

At this point, the absolute error is around a factor of 2 but this can be improved substantially through the use of standard calibration gases. The relative error depends on the particular species, spectral overlap with other species and statistical noise. We have found empirically that the fit error for spectrally isolated species is approximately 5%. These errors are also in close agreement with those determined from a linear least squares fitting routine. For species which overlapped spectrally such as IPA and MEK, the individual errors can be as large as 100%, but the combined error is still on the order of 5%, which translates in this case to a few hundred ppb. Figure 29 shows a plot where the concentration of each component was varied by +/- 10%. The contributions of each species are evident and illustrate the best wavelengths for measurement. In figure 30, the case where both IPA and MEK were present is illustrated. Here, the data were fit either with both IPA and MEK, or just MEK or IPA. It is clear from this plot that the data are fit quite well with either MEK or IPA. Unfortunately, the distinctive peaks of MEK and IPA were masked by strong water vapor absorptions making identification difficult. There are however, some less distinguishing features near 2900 and 3010 cm^{-1} that may be used. Another option is to use a water scrubber but this could introduce uncertainty in other species.

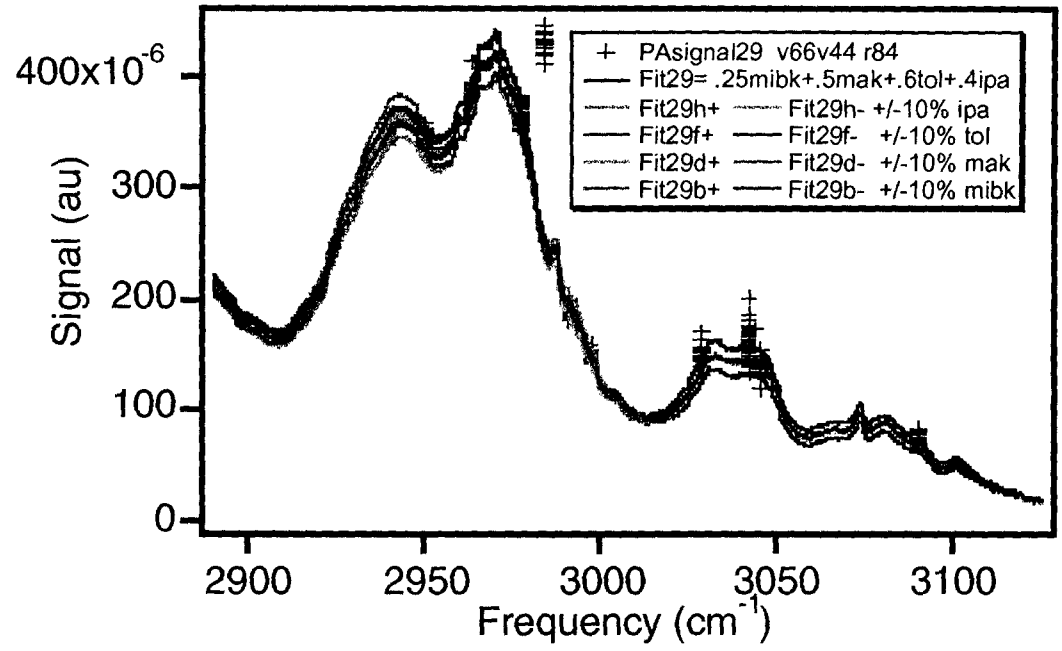

Figure 29. Fit of data made by varying the concentration of each component by +/-10%.

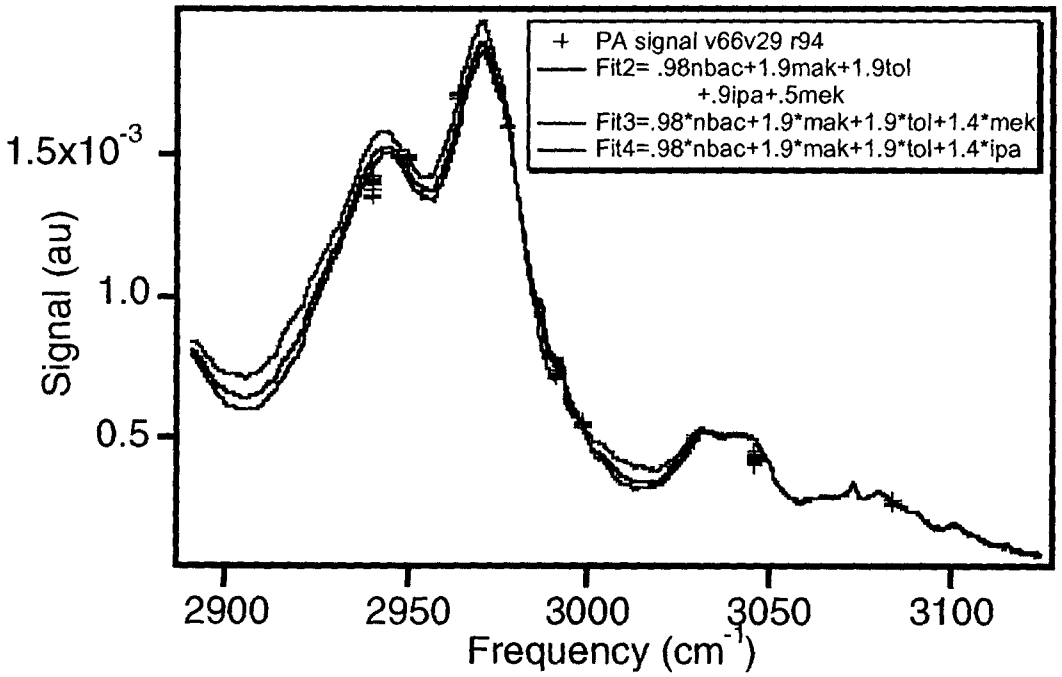

Figure 30. Fit of data in a case where both MEK and IPA were present. The data are fit quite well with either MEK or IPA. Clearly, more wavelengths are required for speciation.

Future Work

Gas Phase Detection

The long term objective of this work is to bring this technology to the point where it is attractive for routine field use. The system would not only have to be competitive with existing technologies but would also have to be more versatile, such as the ability to detect a larger suite of species more rapidly and with higher sensitivity than currently possible. Size, cost, maintenance and reliability are also considerations.

As part of this goal, we are, under another program currently developing a fiber laser replacement for the Coherent IR pump laser. A fiber laser would be significantly smaller and cheaper than the current pump laser. The fiber laser could also have the advantage of pump tuning, resulting in a considerably simpler, more efficient and robust system. The fiber laser is currently under development at the Naval Research Laboratories in collaboration with Sandia National Laboratories. Initial experiments with fiber coupling conducted in our laboratory indicate that due to the improved beam quality associated with fiber pumping, the OPO efficiency is greatly improved. The wavemeter is also a rather large, costly component of the system. Recently however, extremely compact, low cost wavemeters have become available through the telecommunications industry. There are also improvements that could be made to the photoacoustic cell. Since the sensitivity scales inversely with diameter and directly with length, the cell geometry could be modified, yielding an increase in sensitivity of a factor of two or more. In addition to improved sensitivity, the calibration of the cell needs to be more accurately determined using true calibration gases.

Finally, there is also a drive to improve both sensitivity and selectivity by extension to the long wave IR. As shown below in figure 31, the absorptions of many organics are significantly stronger (5-10) and more distinctive in the long wave (8-12 μm) region. Recent advances in nonlinear optical materials offer the potential of PPLN analogs for the long wave IR. This work is currently underway at Stanford, being facilitated in part by funding from Sandia under a DOE NN-20 program.

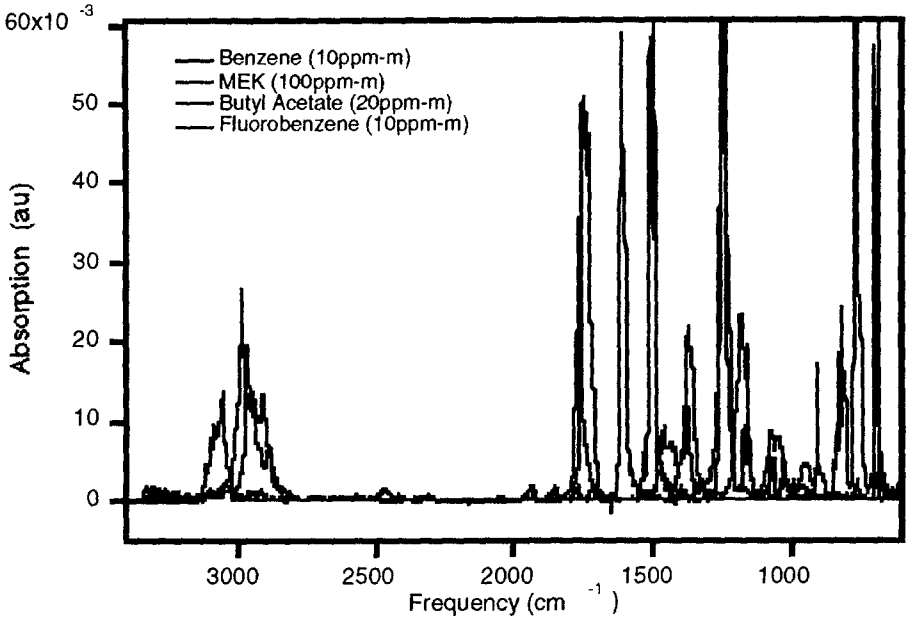

Figure 31. Extension to the long wave IR (8-12μm) region offers the possibility of stronger absorption coupled with better selectivity.

Acknowledgments

The authors would like to acknowledge the SERDP office for their continuous and generous support of this project. We would also like to acknowledge the many people who have contributed to this project. We thank Karla Armstrong for her technical support of the PPLN laser, photoacoustic system, field test and data reduction, Larry Thorne and George Buffleben for their analytical analysis of gas samples, George Sartor for mechanical support, and Tom Kulp for his many hours of technical assistance and support. We also acknowledge Chris Harvey from LLNL who also provided analytical analysis of the stack gas samples. Finally, we acknowledge support from the DOE, Office of Nuclear Nonproliferation, the Gas Research Institute and Coherent Laser Group for without the close synergy of these projects and collaborations we would not have made as much progress.

References

1. A. Balakrishnan, S. Sanders, S. DeMars, J. Webjorn, D. W. Nam, R. J. Lang, D. G. Meyhuys, R. G. Waarts, and D. F. Welch, Opt. Lett., **21**, 952, (1996).

2. S. Sanders, R. J. Lang, L. E. Myers, M. M. Fejer, and R. L. Byer, Electron. Lett., **32**, 218, (1996).

3. W. R. Bosenburg, A. Drobshoff, J. I. Alexander, L. E. Myers, and R. L. Byer, Opt. Lett., **21**, 1336, (1996).

4. K. Schneider, P. Kramper, S. Schiller, and J. Mlynek, Conference on Lasers and Electro-Optics, Postdeadline paper CPD26, May 1997.

5. L. E. Myers, R. C. Eckardt, M. M. Fejer, R. L. Byer, W. R. Bosenburg, and J. W. Pierce, J. Opt. Soc. Am. B, **12**, 2102, (1995).

6. P. E. Powers, Thomas J. Kulp, and S. E. Bisson, " Continuous tuning of a CW periodically-poled lithium niobate optical parametric oscillator by use of a fan-out design," Opt. Lett., **23**, 159-161 (1998)

7. D. D. Nelson, A. Schiffman, K. R. Lykke, and D. J. Nesbitt, Chem. Phys. Lett., **153**, 105, (1988).

8. R. Gerlach and N. M. Amer, Appl. Phys. **23**, 319-326 (1980)

9. P. L. Meyer and M. W. Sigrist, Rev. Sci. Instrum. **61**, 1779-1807

10. F. Harren and Jorg Reuss, **Photoacoustic Spectroscopy** in Encyclopedia of Applied Physics, VCH Publishers, **19**, 413-435, (1997)

11. F. G. C. Bijnen, F. J. M. Harren, J. H. P. Hackstein, and J. Reuss, " Intracavity CO laser photoacoustic trace gas detection: cyclic CH_4 H_2O and CO_2 emissions by cockroaches and scarab beetles," Appl. Opt. **35**, 5357-5367 (1996)

Real-Time Measurement of Metals by Laser-Induced Plasma Spectroscopy

Executive Summary

A novel laser-induced plasma spectroscopy (LIPS) has been developed for continuous emission measurement of toxic metals and particulate matter. The innovative design of the aerosol spectrometer has been submitted for patent application by the Oak Ridge National Laboratory (*DOE/Lockheed Martin Energy Research Corp. Invention Disclosure No. ERID0706, S-92, 560*) in May 1999. Operational parameters including the laser wavelength, laser energy, and the use of aerosol beam focusing technique were examined in the design. It was found that more laser energy input to producing plasma could produce a higher LIPS signal. The UV energy (266-nm) could couple with aerosol material more efficiently than the IR (1064-nm) energy in creating plasma. Multiphoton ionization mechanism was found to dominate the plasma ignition when the UV light was used. On the other hand, thermal ionization was the primary mechanism initiate plasma by the 1064-nm wavelength. The green (532-nm) energy was selected as the operating wavelength in the design of field portable LIPS due to almost equal contribution from both multiphoton and thermal ionization mechanisms in initiatiating plasma. Furthermore, with the coupling of a real-time aerosol mass concentrator like the aerosol beam focusing device developed in this project, the amount of laser energy (at 532-nm) required to initiate plasma could be further reduced. This lends a small laser configuration well suited for field operation. The experimental data also showed that the LIPS signals were regulated by the SERDP aerosol beam-focusing (ABF) device that provides a precise control on the delivery of aerosol mass thus permitting quantitative determination of aerosol metal content. This has not been reported previously in the literature and had remained a problem for a long time when performing quantitative analysis using the traditional LIPS technique. It was also found in this study that the LIPS technique itself was insufficient to detect trace metals in aerosol at a level comparable to those found in source emissions. This is due to the discrete nature of aerosol mass distribution inside a source, a property that is unique to aerosol sample. By coupling an aerosol beam-focusing technology, we have enhanced the LIPS sensitivity by more than 250% with reduced laser energy requirements. A rugged compact ABF-LIPS spectrometer was successfully developed. Finally, the laser-induced plasma spectroscopy was proven to be a non-species specific analysis. The ABF-LIPS technique measures the true total elemental composition associated with aerosol rather than the concentration of speciated metals. To measure speciated metals associated with aerosols in real-time and *in-situ* at source emissions, other techniques have to be developed.

BACKGROUND

Continuous *in-situ* measurement of aerosols, when feasible, is the preferred option for data collection in many applications; e.g., scientific research, regulatory compliance, environmental monitoring, engineering control, and decision making. Rapid detection is required, for instance, to provide data for understanding some chemical reaction kinetics and for diagnosing the performance of an internal-combustion engine. Continuous emission monitoring, as another example, may be needed to provide data for real-time engineering control of the emissions of hazardous air pollutants and to meet future regulatory requirements. In reality, however, many technical difficulties are present for continuous measurement. Fluid conditions of a source emitting toxic metals can be hot, humid, and/or corrosive thus creating problems for instrumentation.The toxic metals include arsenic, beryllium, cadmium, nickel, mercury, selenium, vanadium, radionuclides, and their organo-metallic species that could be more toxic in terms of bioavailability than their elemental forms. Many metals can be found in the aerosol phase with elemental mercury being the only exception. Most reactive mercury and organo-mercury species are found in aerosol. To measure aerosol and the elemental composition of the particles in a source environment one traditionally employs a filter-pack sampling train followed by instrumental analysis in a laboratory. This practice has several inherent problems that include (1) bias due to sampling, (2) error due to sample handling, and (3) collection of non-representative data due to inadequate number of samples. The sampling bias could result when conditions inside a source (e.g., a stack) are different from the ambient conditions where the samples are taken. Particle nucleation, agglomeration, and coagulation can alter particle size distribution and chemical composition leading to inaccurate data when sample dilution is employed. The sample handling errors could be human errors that are common even for a skillful technician. The cost involved in source sampling and analysis is high that prohibits the collection of a large number of samples. A small sample number may not be adequate to fully describe the source emission and its temporal variation making the data less representative. Furthermore, for hazardous sources the samples are better contained inside without being drawn to the ambient. These factors have encouraged development of continuous emission measurement techniques for emission sources.

A number of instrumental techniques currently exist for the measurement of trace elements associated with airborne particulate matter or aerosols (Hopke, 1985). These include X-ray fluorescence (XRF), proton-induced XRF, inductively coupled plasma emission spectroscopy, instrumental neutron activation analysis, and graphite-furnace atomic absorption spectroscopy, to name a few. To meet the requirements of developing a one-person field portable and rugged instrument for continuous aerosol measurement, the laser-induced plasma emission spectroscopy (LIPS) was found to be the best candidate among several promising techniques (Martin et al. 1999). The laser-induced plasma spectroscopy technique requires *no* alteration of sample condition, because the measurement is done *in-situ*. The short cycle time (~ 100 ms) between each measurement makes the LIPS observation nearly *real time*.Laser-induced plasma

spectroscopy, also called laser-induced breakdown spectroscopy, has been investigated for a large number of chemical analyses (Aragon *et al.* 1993; Belliveau *et al.* 1985; Cheng, 1999; Grant *et al.* 1991; Kirchheim *et al.* 1976; Martin et al., 1999; Millard *et al.* 1986; Niemax and Sdorra, 1990; Neuhauser *et al.*, 1999; Panne et al., 1998a & 1998b; Radziemski *et al.* 1983; Simeonsson and Miziolek, 1994; Wisbrun *et al.* 1993; Yalcin et al. 1996). Applications of LIPS have been limited due to insufficient analytical performance compared to other commonly used atomic emission spectrometric techniques such as inductively coupled plasma/atomic emission spectroscopy (ICP/AES). The LIPS technique however has several advantages over the other traditional analytical techniques. These advantages include the rapid turn-around time, non-intrusive, *in-situ*, flexible probe configuration, and availability as a compact trace metal analyzer. These strengths make LIPS a suitable candidate for the development of a small-footprint field-portable multi-element monitor to be used in hazardous environment such as a radiological hot cell, mix-waste contaminated area, and high-temperature combustion chamber.To raise the analytical performance of LIPS a number of techniques had been tested, although none was directed specifically toward aerosol measurements. Sattmann *et al.* (1995) demonstrated the use of double or multiple laser pulses to achieve higher signal-to-noise ratio for detecting Si in solid steel samples. They found double pulses enhanced the signal over single pulses used in traditional LIPS by 2 orders of magnitude. Gornushkin *et al.* (1997) suggested the use of LIBS/laser-excited atomic fluorescence spectrometry technique for the determination of cobalt in solid matrices: graphite, soil, and steel. They found this combination technique to have linearity over 4 orders of magnitude in the ppb to ppm range, and the result was comparable to ICP/AES. These interesting techniques are harder to develop for a field-portable, rugged unit using current laser and gated detector technologies than a single-shot LIPS technique. Furthermore, they have not been tested on aerosol samples. Thus, alternative designs were pursued to improve LIPS performance for aerosol measurement. In this paper, we will demonstrate that the sensitivity of single-pulse LIPS for aerosol measurement can be significantly improved by a new probe configuration called "Aerosol Beam Focusing" (ABF). The ABF technique was adopted from a similar design by Fernandez de la mora and Riesco-Chueca (1988).

Laser-Induced Plasma Spectroscopy (LIPS)

The laser-induced plasma spectroscopy is fundamentally an emission spectroscopy. The major differences between LIPS and other emission spectroscopy such as the Inductively Coupled Plasma or the Microwave-Induced Plasma are (1) exceedingly high activation energy and (2) the pulsed nature of the activation energy from the laser source. In LIPS, a pulsed laser beam is tightly focused onto an aerosol sample. If the diameter of the focal spot were 30 μm, the focal volume of the sphere is on the order of 10^{-8} cm^3. Given a 6-ns laser pulse emitting 100 mJ per pulse, the laser energy in this focal volume could reach 2,000 GW cm^{-2} creating plasma whose core temperature exceeds 20,000 K and peak electron density exceeds 10^{12} per cm^{-3}. This creates a micro-plasma of approximately 2

mm in diameter with its peak temperature 4 to 5 times higher than that of other plasma emission spectroscopy (e.g., the inductively-coupled plasma spectroscopy).Material inside the LIPS plasma would be atomized. Atoms would be excited. Excited atoms release light at their characteristic wavelengths as they relax from the plasma-excited states. The emission light generally lasts for approximately a few nanoseconds to few microseconds. At a few nanoseconds away from the plasma ignition one can observe only the bright broadband light generally known as the *Bremsstrahlung*. Fine line structure will gradually appear in addition to the "fast decaying" broadband light background later. Typically in the range of a few microseconds after plasma ignited, the broadband emission background will significantly subside. The fine line structure of a spectrum resulting from the emission from excited elements will then become prominent. The pattern and duration of an emission light at a specific wavelength depends on several factors such as the atomic species, the surrounding ionic cloud and gas, and the laser characteristics (e.g., wavelength, pulse-length, and energy). These factors together determine the physical characteristics of the plasma. The time-resolved LIPS technique takes advantages of the time-dependent spectral pattern that is specific to an atom to improve the detection and sensitivity of LIPS.A high-resolution spectrograph and an intensified charge coupled device (ICCD) was used to collect the emission light for the LIPS spectrochemical analysis. The identified wavelengths of an atom was compared to an atomic spectroscopic library obtained from the National Institute of Science and Technology (NIST reference database 38, the Spectroscopic Properties of Atoms and Atomic Ions Database) that provides standard spectrum for qualitatively determining the identity of the atom. The background corrected photon counts were recorded and evaluated against a calibration curve to quantitatively determine the amount of the element in the aerosol sample. The calibration curve was established for this study using prepared solutions of known concentrations.

Experimental Setup

The basic laboratory configuration of the aerosol beam-focused - LIPS experiment is shown in Fig. 1. A high-power pulsed laser such as a Q-switched Nd: YAG laser emitting at 532-nm was used as the excitation source. This coherent monochromatic light was tightly focused to a small focal volume inside the sample cell to create a plasma. The emission light of the plasma was collected and analyzed by a spectrograph consisting of 3 gratings (2, 1200 grooves/mm and 1, 300 grooves/mm) and an ICCD of 1024x256 micro pixel array. This detection configuration yields a spectral resolution approximately 0.05 nm at wavelength of 435.8 nm. The resolution is defined by the full width at the half maximum at 435.8 nm with 10-μm slits. When the laser fires, it also sends a digital trigger signal, which was approximately 5V, to a delay function generator that was programmed to postpone the opening of the detector for a pre-selected time interval.

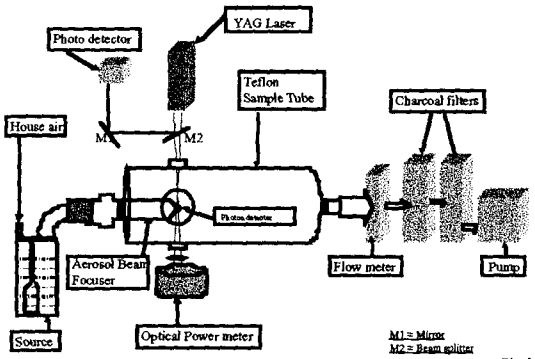

Fig. 1

The delay generator then sends a second digital signal to the spectrometer for the retrieval of emission light after the clock reaches the pre-programmed time interval. The pulse-length of our laser was 6 ns and the nominal power intensity for the 532-nm wavelength used was around 100 mJ. The energy could be varied continuously from 50 to 240 mJ per pulse. Aerosol particles generated by the atomizer are pumping through the aerosol beam focuser and are focused into a spot of diameter approximately 100 μm smaller than the diameter of the plasma induced by the high-power laser. The digital delay function has been coded in LabVIEW and to run on the portable computer. In addition to 532-nm light source, we also conducted the LIPS experiments using wavelengths of 1064 and 266 nm of the Nd: YAG laser to understand how wavelength affects the LIPS signal under ABF and non-ABF configurations.

High-resolution spectrum obtained via the SERDP ABF-LIPS technique

A screen-capture of the emission spectrum of chromium in aerosol is shown in Fig. 2. The number median diameter of the aerosol was approx. 300 nm and the geometric standard deviation was 1.29. The number density approximately 10^6 cm^{-3} at 300 nm. The aerosol chromium concentration was 98 ng m^{-3}. The excitation wavelength was 532 nm. The delay time used for this detection was 18 μs after the laser was fired and the gatewidth was 8 μs. The presence of the wavelength triplet at (425-nm, 427-nm, & 429-nm) is essential for a positive identification of the aerosol chromium. The wavelength triplet did not appear until about 16 μs delay and last for only 10 μs. This and the pre-scribed delay times are two required criteria built into our detection algorithm to eliminate possible spectral interferences from emissions from other atomic species such as iron, commonly present in environmental samples. The 425-nm line of the triplet was used to quantitatively determine the amount of chromium in aerosol. A total of 1000 shots (= 1000*0.1 = 1 minutes and 40 seconds) were used to yield this measurement at the aerosol chromium concentration of 100 ng m^{-3} shown in the figure.

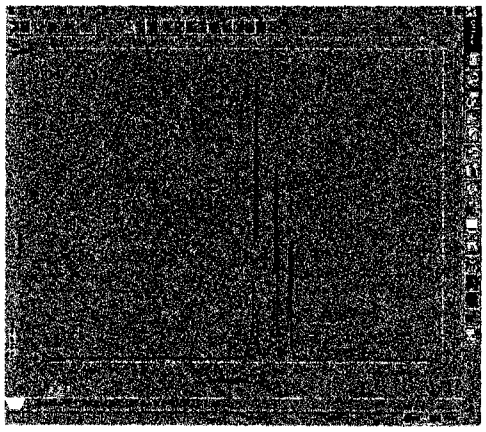

The analytical problem associated with the LIPS technique encountered in previous studies (Haas et al. 1997; Hahn et al. 1997; Dunn et al. 1998) was related to the

uncertainty of *in-situ* aerosol particle sampling. Without a means to introduce aerosol material to the LIPS focal volume as in previous studies, the LIPS technique had suffered at least two types of sampling uncertainty. One of which is related to the stochastic nature of aerosol distribution, and the other is the "plasma efficiency" which is the percentage of laser shots that are successfully hitting aerosol particles.

Aerosol Beam Focusing Nozzle

A significant development in FY99 was the addition of an aerosol beam focusing device or nozzle to the LIPS instrument. The purpose of aerosol focusing is not to collimate the particles into a straight line as required by the laser ablation mass spectrometry (Silva et al. 1999) or ion-trap (Reilly et al. 1997) single particle analysis, but to concentrate particles to a point smaller than the size of the plasma. A simplified schematic drawing of the focusing nozzle used in the experiment is shown in Fig. 3a. A properly operated focusing nozzle effectively concentrates particles increasing the efficiency of material delivery to the plasma core and improves the odds for successful laser shots. This improvement is significant as shown in the following section and critical for the development of a highly sensitive field-portable LIPS aerosol spectrometer.

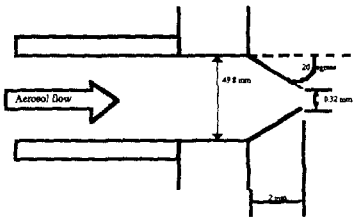

Figure not for scale. Size of a plasma about 2 mm in diameter.

Fig. 3a

A flow velocity simulation result for the nozzle of the geometry shown in Fig. 3a using a commercially available computational fluid dynamics code is shown in Fig. 3b. The focal length of the nozzle was approximately 2.4 mm from the exit and the focal point cross section was about 50 micrometers. The flow downstream from the nozzle exit was operating at about 2.5 l min^{-1}. This creates a negligible pressure drop across the nozzle exit and minimizes any possible damage to the particle integrity without losing the focusing capability. The flow was maintained within sub-sonic regime. This simple nozzle works equally well compared to a few other complicated configurations under the subsonic focusing conditions. No sheath air was used in this design, additional tests (results not shown here) indicate that the use of sheath air did not improve our spectrochemical analysis. A detailed comparison and characterization of different nozzle geometries and operating conditions with respect to the LIPS detection is presented in another paper currently in preparation.

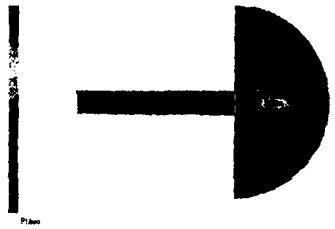

Fig. 3b

Effects of Aerosol Beam Focusing Configuration on LIPS

Comparison of LIPS results between with and without aerosol beam focusing is presented in Fig. 4a. The aerosol chromium concentration was maintained constant at 100 ng m^{-3} so we could examine the focusing effects. The 532-nm wavelength was used and a total of 1,000 shots were recorded. The energy levels of 3 bar pairs were at 50, 75, and 250 mJ per pulse. At the 50-mJ level, we collect no quantifiable signals defined as the signal where its Signal-to-Noise (S/N) ratio ≥ 2 from the 1,000 shots. The signal (S) is taken as the Background Correct Counts (BCC) at 425.5 nm, and the noise (N) is computed as follows:

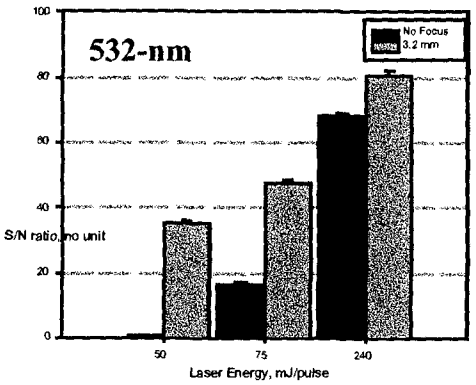

Fig. 4a

$$N = \sqrt{(N_r^2 + N_d^2 + N_s^2)}$$

Where N is the total noise for a measurement, N_r^2 is the ICCD pixel readout noise in counts, N_d^2 is the electronic dark current noise in counts, and N_s^2 is the shot background noise in counts at a selected wavelength representing the background (i.e., 432 nm in this case). The S/N ratio is then obtained by dividing the value of S by that of N.

When a 3.2-mm nozzle exit size was used, we could detect the chromium and the S/N ratio was registered at 35 ± 0.7 as a results of the 1,000-shot. Where the laser energy was increased one could in practice ignite plasma and generate LIPS signal at low particle mass as shown in this figure. The ratio for the non-focusing cases goes from 17 ± 0.3 at 75 mJ to 68 ± 1.4 at 250 mJ. The S/N ratio for the focusing cases goes from 47 ± 1.0 at 75 mJ to 81 ± 1.6 at 250 mJ. The increases of the S/N ratios from non-focusing to focusing configuration were significant. Note that the increase in the S/N ratio for the non-focusing configuration from 50 to 250 mJ appears to be a non-linear function of laser energy. This could be due to significant variation in the amount of the material present inside the plasma. The focusing configuration produces a linear relationship between the S/N ratio and the laser excitation energy input indicates that the focusing nozzle maintains a rated material supply to the plasma that enables a precise quantification using LIPS.

Selection of Optimal Laser Wavelength on ABF-LIPS

A similar bar chart is presented in Fig. 4b for the 266-nm wavelength laser energy. All operating conditions remain fixed except the wavelength. The 2 bar pairs were for 50 mJ and 75 mJ, respectively. The maximum laser energy at 266-nm we could obtain from this laser was around 80 mJ/pulse. We noticed that no LIPS signal could be obtained

without the focusing nozzle at 50-mJ energy using the 266-nm wavelength. The detection became possible when 75-mJ of energy was used in the non-focusing case.

Also note that the S/N ratio was 17 for the 532-nm using 75 mJ, while the ratio was now greater than 50 for 266-nm wavelength in the same non-focusing configuration. This could be due to different ionization mechanisms postulated for the 266-nm wavelength that was mostly multiphoton ionization, while at the 532-nm both the multiphoton and thermal cascade ionization were present (Martin et al. 1999). The increase of the S/N ratio as a function of the 266-nm laser energy in the energy range [50,75] mJ/pulse was minimal as compared to that at the 532-nm. If the coupling of energy to matter via multiphoton ionization saturated with the amount of material inside the plasma, the linearity as seen in Fig. 4a would not be present in Fig. 4b. This result also indicates that 266 nm would not be a good choice of wavelength to use in the source emissions measurement that generally have high concentration, although it did provide a better S/N ratio compared to the 532-nm wavelength in both focusing and non-focused configurations in our study.

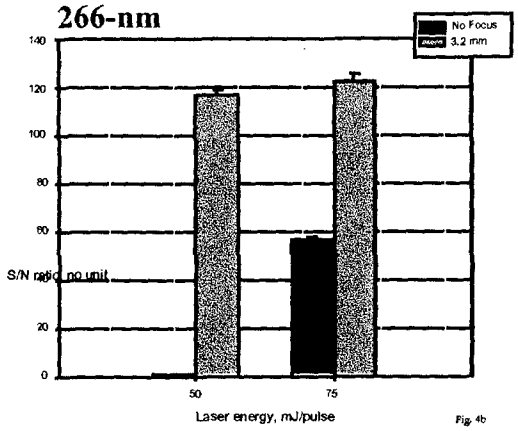

Fig. 4b

The pattern of the S/N ratios of the 1064-nm laser energy chart shown in Fig. 4c are similar to that of Fig. 4a (532-nm) and 4b (266-nm), in which high laser energy produces a higher S/N value. Studies by Radziemski et al. (1983) and Martin et al. (1999), for example, noted that most of the LIPS signal from the interaction of the 1064-nm wavelength with aerosol was resulted from the thermal cascade ionization. Our results displayed in Fig. 4c show that the LIPS signal might not be a linear function of laser energy as we previously thought. For instance, the S/N ratios (Fig. 4c) for the focused cases level off when the laser energy is increased from 200 mJ per pulse to 400 mJ. This behavior is inconsistent with those seen in the other two wavelengths where more energy leads to higher S/N ratio. Remember that the plasma shielding phenomenon (Liu et al., 1999), which plasma shield more laser input energy thus creating a plateu of optical signals to be detected, may not be an issue here because the sample matrix is a dilute aerosol system rather than a bulk solid sample. Thus, the amount

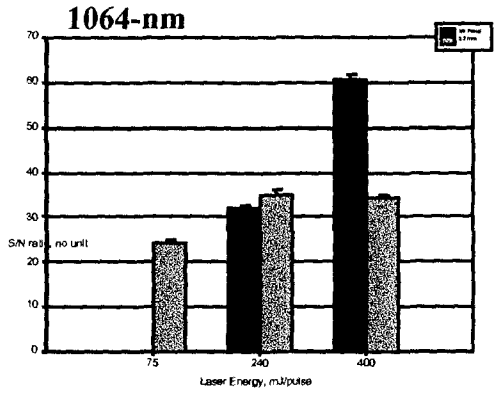

Fig. 4c

of material inside a plasma volume would not create a dense plasma to cause a plasma shielding problem.

However, the laser energy inputs of the 1064-nm in this experiment were about twice to four-time higher than that of the 532- or 266-nm. This result shows that using more laser energy cannot possibly produce more signals exceeding what is available from the material inside the plasma. On the other hand, more laser energy leads to a higher S/N ratio in the non-focusing case consistent with those non-focusing cases in Fig. 4a and 4b. However, high laser energy used in laser-induced plasma generation produces a larger plasma volume as was documented many times in the literature as early as Radziemski et al. (1983). This raises a question regarding the analytical measure of the LIPS measurement. In other words, if the analyte quantity cannot be controlled as in the non-focusing case, the LIPS signal would have to be normalized somehow at the different excitation energy levels for an unknown (or uncontrollable) analyte mass. That can be quite challenging in a field operation. Based on the S/N ratios of the focused result, we found this was not a problem when the focusing nozzle was acting as a mass flow regulator that controls the delivery of aerosol mass to the plasma.

Effects of Chemical Speciation on ABF-LIPS

The ratios of background corrected photon counts (BCC) for chromium (VI) to chromium (III) are shown in Fig. 5. The tri-chromium chloride salt [$CrCl_3$] provided the Cr (III), while the hexachromium salt ($Na_2Cr_2O_7$) provided Cr (VI) for LIPS analyses. Two solution concentrations were used, 4.8 and 11.5 M. The objective of this experiment was to test if ABF-LIPS result is matrix or molecule dependent. The ratio of BCC of the aerosol that was made from the hexachromium salt to that of the tri-chromium salt should be approximately 2 at both molar concentrations, because there are 2 chromium atoms in the aerosol made of $Na_2Cr_2O_7$ while only one is in the $CrCl_3$ aerosol. We show in Fig. 5 that the LIPS signals are consistent with the ratio of 2, and the LIPS can precisely quantify irrespective of the wavelength used. We did not convert this solution concentration to aerosol concentration as in ng m^{-3} as we did in other experiments for the sake of simplicity. When the solution concentration increased from 4.8 to 11.5 M, the BCC ratios of the 1064- and 532-nm wavelength are different. While the 532-nm wavelength still yields a ratio close to 2, which is the correct number, the 1064-nm wavelength configuration yields a higher ratio around 2.35 that is 17% higher than 2. The uncertainty of the ratios was on the order of

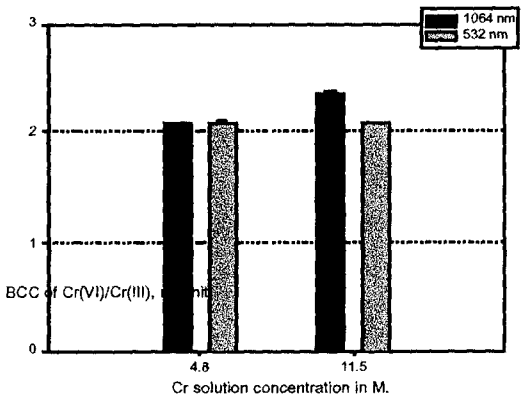

Fig. 5

0.03, so 17% deviation is significant. We currently do not know what caused this discrepancy but hypothesize that the 1064-nm wavelength may be more sensitive to the plasma optical thickness than the 532-nm. As more material present inside the plasma as in the case of 11.5 M, the thermal cascade ionization tends to depend more on the material mass present thus activating the same chromium atoms more than once. Since the repetitive collision of photons with the same atoms has a small probability, one would not expect a substantially higher (on the order of magnitude type) BCC ratio. These results demonstrate that ABF-LIPS does not speciate but it provides a true total elemental concentration in the aerosol sample.

CONCLUSIONS OF LIPS FY99 REPORT

Aerosol beam-focused laser-induced plasma spectroscopy was employed as the principle in the design of a field-portable instrument for the measurement of trace metals associated with airborne particulate matter. Operational parameters examined in the design phase included the laser wavelength, laser energy, and the use of aerosol beam focusing. It was found that more laser energy used in plasma generation could produce a higher LIPS signal. However, the optimal or maximum signal appears to be regulated by the focusing nozzle that provides a precise control for quantitative determination of aerosol metal content. It was also found in this study that the LIPS technique alone, without ABF, was insufficient to detect trace metals (e.g., mercury and chromium) in aerosol at a level comparable to those found in source emissions. This is due to the discrete nature of aerosol mass distribution inside a source, a property that is unique to aerosol sampling. By coupling an aerosol beam-focused technology, we have enhanced the LIPS sensitivity by more than 250% and consuming much less laser energy than previously needed. A rugged compact aerosol beam-focusing laser-induced plasma spectrometer was successfully developed. Finally, laser-induced plasma spectroscopy was proven to be a non-species specific analysis. The ABF-LIPS technique measures the true total elemental composition associated with aerosol rather than the concentration of speciated metals. To measure speciated metals associated with aerosols in real-time and *in-situ* at emissions, other techniques have to be developed.

REFERENCES

1. Aragon, C., Aguilera, A. J., and Campos, J. (1993) *Appl. Spectrosc.* 47,606.

2. Belliveau, J., Cadwell, L., Coleman, K., Huwel L., and Griffin H. (1985) *Appl. Spectrosc.* 39,727.

2. Cheng, M. D. and Martin, M. Z. (1998) DOE FETC Air Quality Conference.

3. Cheng, M. D. (1999) *Fuel Process. Technol.* in press.

4. Dunn, J. E., Sallie, R., Gibson, L. V., Kinner, L. L., Peeler, J. W., and Shigehara, R. T. (1998) *Field Test to Determine Deployment Potential of Three Candidate Multi-Metals Monitoring Techniques at the Toxic Substances Control Act Incinerator*, Final Report, Bechtel Jacobs, BJC/OR-27.

5. Fernandez de la mora, J. and Riesco-Chueca, P. (1988) *J. Fluid Mech.* 195, 1-21.

6. Gornushkin, I. B., J. E. Kim, B. W. Smith, S. A. Baker, and J. D. Winefordner (1997) Determination of Cobalt in Soil, Steel, and Graphite Using Excited-State Laser Fluorescence Induced in a Laser Spark, *Appl. Spectrosc.* 51(7): 1055-1059.

7. Grant, K. J., Paul, G. L., and O'Neill, J. A. (1991) *Appl. Spectrosc.* 45, 701.

8. Haas, W. J., Bergan, N., Brown, C. H., Burns, D. B., Lemieux, P. M., Priebe, S. J., and Ryan, J. V. (1997) *Performance Testing of Multi-Metal Continuous Emissions Monitors*, Final Report to US Department of Energy, November 17, IS-5128, UC-606.

9. Hahn, D. W., W. L. Flower, and K. R. Hencken (1997) *Appl. Spectrosc.* 51(12), 1836.

10. Hopke, P. K. (1985) *Receptor Modeling*, John Wiley & Sons, New York, NY.

11. Kirchheim, R., Nagomy, U., Maier, L., and Tolg, G. (1976) *Anal. Chem.*, 48, 1505.

12. Liu, H. C., X. L. Mao, J. H. Yoo, and R. E. Russo (1999) *Spectrochimica Acta Part B.*, 54: 1607.

13. Martin, M. Z., Cheng, M. D., and Martin, R. C. (1999) *Aerosol Sci. Technol.* 31(6): 409.

14. Millard, J. A., Dalling, R. H., and Radziemski, L. J. (1986) *Appl. Spectrosc.* 40, 491.

15. Neuhauser, R. E., U. Panne, R. Niessner, and P. Wilbring (1999) *Fresenius J. Anal. Chem.* 364:720-726.

16. Niemax K., and W. Sdorra (1990) *Appl. Opt.* 29: 5,000.

17. NIST standard reference database number 38. NIST Spectroscopic Properties of Atoms and Atomic Ions Database originally prepared by the National Research Council Committee on line spectra of the elements under the editorship of: J. Reader and C. H. Corliss. Database software developed by W. G. Mallard, G. R. Dalton, J. W. Gallagher.

18. Panne, U., C. Haisch, M. Clara, and R. Niessner (1998a) *Spectrochimica Acta Part B.* 53:1,957-1,968.

19. Panne, U., M. Clara, C. Haisch, and R. Niessner (1998b) *Spectrochimica Acta Part B.* 53:1,969-1,981.

20. Radziemski, L. J., Loree, T. R., Cremers, D. A., and Hoffman, N. M. (1983) *Anal. Chem.* 55, 1246.

21. Reilly, P. T. A., Gieray, R. A., Yang, M., Whitten, W. B., and Ramsey, J. M. (1997), *Anal. Chem.*, 69(1): 36-39.

22. Sattmann, R., Sturm, V., and Noll, R. (1995) *J. Phys. D: Appl. Phys.* 28, 2181-2187.

23. Silva, P. J., Liu, D. Y., Noble, C. A., and Prather, K. A. (1999) *Environ. Sci. & Technol.*, 33(18): 3068-3076.

24. Simeonsson, J. B., and A. W. Miziolek (1994) *Appl. Phys.* B, 59, 1.

25. Wisburn, R., Niessner, R., and Schroeder, H. (1993) *Anal. Methods Instrument.* 1, 17.

26. Yalcin, S., D. R. Crosley, G. P. Smith, and G. W. Faris (1996) Spectroscopic Characterization of Laser-Produced Plasma for In Situ Toxic Metal Monitoring, *Hazardous Waste Hazardous Materials*, 13(1): 51.

ACCOMPLISHMENTS in FY1999

1. Designed and tested several aerosol beam-focusing devices and configurations. These devices were operated under different sampling conditions - pressure drop, flow rate, nozzle height, and convergence boundary geometry in the laboratory. One focuser presented in this report, which produce satisfactory results during the tests, was chosen as the final design for the field portable prototype.

2. Completed system integration for the field portable ABF-LIPS into a breadboard, which when boxed, has a physical dimension no bigger than the size of a carry-on luggage that weights less than 50 lbs.

3. Calibrated the ABF-LIPS against aerosol particles of known chemical composition and sizes. A vibrating orifice aerosol generator was used to produce the particles of narrowly defined particle sizes ($\sigma_g = 1.09$). The system produces precise responses as expected. The data are still being analyzed and the analysis result will be submitted for journal publication.

4. The Lockheed Martin Energy Corporation (the manager of Oak Ridge National Laboratory for DOE) filed a patent for the ABF-LIPS design. The invention is protected. Several manuscripts have been prepared for submission to journals for peer-review. One copy of those published had been forwarded to the program office.

ACKNOWLEDGEMENTS

The research was funded by the Strategic Environmental Research and Development Program jointly administrated by the US Department of Defense, Department of Energy (DOE), and the Environmental Protection Agency. Dr. Madhavi Martin has assisted in setting up and performing the LIPS experiments. Dr. Thomas Wainman assisted in assembly of the field portable systems on a breadboard, and Dr. Da-Ren Chen from the University of Minnesota provided assistance in the design and validation (computationally and experimentally) of the aerosol beam focusing nozzle. A portion of this research was also funded by the Natural Gas and Oil Technology Program Office of the DOE Fossil Energy Program. The Oak Ridge National Laboratory was managed by Lockheed Martin Energy Research Corp. for the U.S. Department of Energy under contract number DE-AC05-96OR22464. The ABF-LIPS is a patent-pending technique developed at the Oak Ridge National Laboratory (US Patent Application No. 09/416,337).